~~The Development~~ SASIEv.1: A framework for seasonal ~~Application of an~~ multi-centennial Arctic ~~Sea Ice Emulator v.1~~sea ice emulation

Sian Megan Chilcott [1,2] and Malte Meinshausen [1]

[1]School of Earth and Atmospheric Science, The University of Melbourne, Parkville 3010, Victoria, Australia

[2]Max-Planck-Institute for Meteorology, Universität Hamburg, Hamburg, 20146, Germany

Correspondence: Sian Megan Chilcott (smchilcott@student.unimelb.edu.au)

Abstract. The high computational expense of complex climate models and their tendency to underestimate observational records of Arctic sea ice sensitivity to anthropogenic forcers, challenge our ability to assess the magnitude of forcing that will cause Arctic sea ice loss to cross critical thresholds. To address these limitations, we ~~development an~~ develop a parameterisation framework, SASIEv.1, to emulate Arctic sea ice~~emulator~~, that is calibrated to the response of sea ice area to global warming in physically-based CMIP6 models and constrained to observations. Our constrained ~~emulator~~ framework reduces the remaining budget of CO_2 that can be emitted ~~to prevent~~ while preventing seasonally ice-free conditions from 821GtCO_2 by CMIP6 multi-model ensemble estimates to 380GtCO_2. This suggests that limiting global warming to 1.5°C is sufficient to prevent a seasonally ice-free Arctic Ocean, whereas 2°C proves insufficient. Our results also provide insight into the future of winter sea ice over a greater ensemble range than previously possible, pinpointing the emission threshold at which the ice pack detaches from land, after which the ice pack rapidly disappears to year-round ice free conditions.

1 Introduction

Arctic sea ice forms a complex yet fundamental component of the Earth system and is a sensitive indicator of global climatic changes. Since the satellite record began in 1979, the September ice pack has declined by more than 13% per decade in response to anthropogenic greenhouse gas emissions (Serreze and Stroeve, 2015).

Global climate models (GCMs) used in the most recent (sixth) phase of the Coupled Model Intercomparison Project (CMIP), are the most comprehensive tools we have for predicting how Arctic sea ice will change in the future. Their projections unanimously show continued year-round reductions in Arctic sea ice throughout the 21st century, with the majority of models projecting a seasonally ice-free Arctic Ocean within the next 15 to 50 years, commonly defined as the first time ~~SIA~~ sea ice area (SIA) falls below 1 million km^2 in a given month (SIMIP Community, 2020). Though models agree ice loss will persist into the future, there are large uncertainties surrounding their projections (SIMIP Community, 2020). One conceptually convenient metric to measure changes in sea ice is the 'sea ice sensitivity', which is generally defined as the amount of sea ice area lost per degree of global warming. However, GCMs tend to simulate a lower sensitivity of Arctic summer sea ice loss than has been observed (Mahlstein and Knutti, 2012; Rosenblum and Eisenman, 2017; Niederdrenk and Notz, 2018; SIMIP Community, 2020). Models that do simulate present day rates of sea ice loss also simulate considerably higher global warming than observations suggest (Rosenblum and Eisenman, 2017). This is known as the 'hot model' problem and is used to describe models that project climate warming in response to CO_2 emissions that is much larger than other lines of evidence suggest (Hausfather et al., 2022). Recent observations report the Arctic Amplification, defined as the warming ratio between the Arctic and global temperature, over the satellite period has warmed much faster than in CMIP6 models which tend to simulate a relatively constant Arctic Amplification over the 21st century (Chylek et al., 2022; Rantanen et al., 2022; Douville, 2023; Chylek et al., 2023; Hay et al., 2024).

The majority of CMIP6 models limit runs to 2100 as they are too computationally expensive to analyse large numbers of scenarios over multi-centennial timescales (Balaji et al., 2017). A few studies have utilised the limited number of extended simulations, to analyse the winter sea ice response to warming, using the limited subset of available models with extended simulations to 2300, with particular interest in the possibility of a rapid disappearance of winter sea ice (Armour et al., 2011; Hezel et al., 2014; Bathiany et al., 2016; DeRepentigny et al., 2020; Hankel and Tziperman, 2021, 2023). These studies found that the linear decline of Arctic sea ice with cumulative CO_2 emissions to ice-free conditions exhibited through the summer months breaks down in winter. Arctic sea ice declines at a much slower rate in winter before reaching a threshold at which the amount of sea ice loss per emitted ton of CO_2 rapidly increases. A recent study from Ritschel (2024) attributes the rapid loss of Arctic winter sea ice to the detachment of the ice pack from land. They ~~ascertain~~ find that the detachment of the ice pack from land is linked to the timing of geographic muting, a term introduced by Eisenman (2010) to describe the blocking of the ice pack's expansion through the growth season, due to the presence of land masses surrounding the Arctic Ocean. This mechanism explains the slow decline of winter sea ice initially, as the theoretical retreat of winter sea ice is masked by the coastline. This causes the area of the coast bound ice to change minimally. Once the temperature becomes sufficiently high

45 to prevent the ice pack expanding to the coastline, the ice pack has 'detached' from land and exhibits a higher sensitivity to warming (Ritschel, 2024). As the timing of rapid winter ice loss tends to occur after the end of the 21st century, the lack of extended projections in CMIP6 models prevents a thorough analysis of winter ice loss.

This study therefore ~~aims to address three key gaps in the literature. The first fundamentally seeks to~~ has three key aims. First, we build on and extend ~~the insights we gain~~ insights gained from comprehensive, higher complexity model runs to ~~emulate~~
50 develop a parameterisation framework that emulates the CMIP6 response of seasonal Arctic sea ice area to global warming ~~in all months~~ at a much smaller computational expense. In a second step we ~~aim assess~~ evaluate whether the calibration of our parameterisations to CMIP6 models between 1850 and 2100, capture the non-linearity of winter sea ice when extended to 2300. This validation provides insight into the framework's potential to emulate winter sea ice in models that lack projections beyond 2100. Finally, this study aims to ~~assess~~ investigate whether the sensitivity of sea ice loss to global warming can be constrained
55 to match ~~the observed~~ observations, through bias corrections to the global warming and Arctic Amplification trends. This ~~approach~~ study therefore aims to integrate various lines of evidence to efficiently emulate plausible, long-term projections of SIA under a range of ~~SSP scenarios.~~ scenarios. This approach does not intend to offer a model for "off-the-shelf" use, but a methodology by which we and other users can efficiently investigate seasonal and long-term Arctic sea ice trends using the parameterisations presented.

60 ## 2 ~~Arctic Sea Ice Emulator Setup~~ Framework Overview

2.1 ~~Model Description~~ Overview

~~Our emulator setup~~ The SASIEv.1 (Seasonal Arctic Sea Ice Emulator version 1) framework is separated into two stages which are each comprised of three steps (fig. 1). Stage one involves parameterisation development and calibration to CMIP6 data, while stage 2 constrains our CMIP6 informed parameterisations to observations. Within each stage, step i emulates the
65 Arctic Amplification, converting the global annual mean temperature to the Arctic annual mean temperature ~~.~~ (Sect. 4.2 and 4.2.1). Step ii emulates the Arctic seasonal temperature cycle which converts our emulated Arctic mean temperature to the Arctic seasonal temperature (Sect. 4.3) and is then input into the sea ice parameterisation in step iii ~~. In the~~ (Sect. 4.4). In the second stage, we combine the MAGICC global-mean temperature ensemble (Sect. 3), with our probabilistic constraint on Arctic Amplification in step ii (Sect. 4.2.1), which we then pass through remaining steps to produce constrained, probabilistic
70 projections of SIA to 2300. We use the MATLAB programming software version R2024b to run the SASIEv.1 framework, training the parameterisations on the CMIP6, MAGICC, RCMIP and observational datasets described in Sect. 3. Using this approach, the SASIEv.1 framework can be applied without recalibration across all models listed in Table A1, along with their associated SSP scenarios and ensemble members. The framework's parameterisations can also be calibrated to accommodate CMIP6 models beyond those considered in this study. Given that we emulate the sea ice response with parameterisations that

3

75   smooth out year to year variability, our emulation framework therefore does not attempt to capture the year to year natural variability of Arctic sea ice, rather the long-term median Arctic sea ice response.

3   Data Collection and Processing

In the first stage, parameterisations have been calibrated over the period 1850-2100 against the corresponding first ensemble member of ~~12~~ 13 selected CMIP6 models ~~for the~~ (see Table A1) for the Shared Socioeconomic Pathway (SSP) scenarios

80   SSP5-8.5, ~~SSP 2-4~~SSP2-4.5 and SSP1-2.6 and their historical runs. We chose these scenarios and the calibration period based on the availability of both CMIP6 temperature and SIA projections~~.~~, where at least five models also contained projections to 2300. These five models were selected for framework evaluation, presented in Sect. 5.1. By selecting scenarios that represent both the warmest and coolest projected futures, we ensure that our calibrated parameterisations encompass the full range of SIA responses to temperature. This enables the framework to be applied to intermediate scenarios not explicitly used in

85   calibration, that lie within the bounds defined by the extremes. We also focus our calibration on the first ensemble member only, due to the small long-term variability between ensemble members, we instead focus our calibration on a range of models and scenarios. In the second stage~~we force our emulator with~~, we use the MAGICC 600-member ensemble that has been constrained to represent the IPCC AR6 WG1 global warming projections and their uncertainty (Cross-Chapter Box 7.1, IPCC (2021) AR6 WG1; Nicholls et al. (2021)). ~~We combine the MAGICC ensemble with our probabilistic constraint on Arctic~~

90   ~~Amplification in step ii, which we then pass through remaining steps to produce constrained, probabilistic projections of~~ ~~SIA to 2300. Given that we emulate the sea ice response with parameterisations that smooth out year to year variability, we~~ ~~prioritise the development of our emulator's capability to represent structural variability. Our emulation approach therefore~~ ~~does not attempt to capture the year to year natural variability of Arctic sea ice, rather the long-term median Arctic sea~~ ~~ice response. This is because the contribution from internal processes to the overall variability reduces in long-term sea ice~~

95   ~~projections, while the contribution from structural and scenario variability contribute greater significance to the long-term sea~~ ~~ice projections (Bonan et al., 2021).~~ The observational temperature datasets used to analyse the observed Arctic Amplification were the NASA's Goddard Institute for Space Studies Surface Temperature version 4 (GISTEMP) with a 1200km smoothing radius (Lenssen et al., 2019), the Berkeley Earth temperature dataset (BEST) (Rohde and Hausfather, 2020) and the Met Office Hadley Centre/Climatic Research Unit version 5.0.1.0 (HadCRUT5) dataset (Morice et al., 2021). The HADCRUT temperature

100   range was obtained from the 200 member ensemble. In these datasets, near-surface air temperature is based on a combination of 2m temperature observations over land and sea surface temperature (SST) observations over the ocean. The global mean temperature anomaly is defined as the average temperature across the gridded dataset while the Arctic temperature anomaly counterpart is defined as the average of the area poleward of 65°N. Arctic absolute seasonal temperature observations are downloaded as a time series from the Berkeley product. The six observational northern hemispheric SIA datasets used include:

105   the HadISST NSIDC monthly sea-ice area; HadISST original monthly sea-ice area; Comiso-Bootstrap monthly sea-ice area; NASA-Team monthly sea-ice area; OSI-SAF monthly sea-ice area and the Walsh monthly sea-ice area. Finally, cumulative

CO$_2$ emission projections are taken from the historical fossil fuel and industrial datasets that were used for harmonising IPCC emissions scenarios from the AR6 WG3, RCMIP datasetes (IPCC, 2022; Nicholls et al., 2020). As the cumulative CO2 emission projections begin in 1750, to analyse the remaining carbon budget from 2023 we simply subtract the cumulative CO2 emission in 2023 from the total carbon budget in each ensemble.

3.1 ~~Model Calibration~~

4 Framework Calibration

The calibration routine utilises the Nelder and Mead simplex optimisation method (Nelder and Meadf, 1965; Lagarias et al., 1998), with a termination tolerance of 10^{-6} and a maximum iteration of 1000. We use the residual sum of the squared differences (RSS) for goodness-of-fit (GOF) diagnostics during the ~~optimization~~ optimisation process. This setup iteratively evaluates the calibration factor values to ensure they result in an RSS global minimum between the CMIP6 data (with a running mean of 10 years applied) and the emulated data. The optimisation routine is initialised via a number of preliminary runs to generate a series of starting parameters, by randomly sampling values from a set of user-defined ranges for each parameter. Each calibrated parameter in the final model-specific set is designed to control all months in each model. Tables listing calibrated parameter values for all free variables can be found in the Supplementary (Table. A2 and Table. A3).

4.1 Parameterisation Framework

4.2 Step i: The Arctic Amplification Parameterisation

In stage 1, we force our ~~emulator~~ framework with the global mean temperature anomaly from each of the CMIP6 models used in this study. We split the emulation of the Arctic temperature into two parameterisations- annual (step i) and seasonal Arctic Amplification (step ii). Splitting these processes provides the basis for the observational constraint of annual Arctic Amplification in stage 2 of ~~emulator~~ development.

We find that a simple linear regression between the global and Arctic annual mean temperature anomaly ~~$, tas_{(AAAB)} = \beta \cdot (tas_{(GAB)} - tas_{(G}$~~ over the calibration period is sufficient to emulate the CMIP6 Arctic annual mean surface temperature (fig. 2). ~~Where~~ :

$$tas_{(AAAB)} = \beta_{AA} \cdot (tas_{(GAB)} - tas_{(GREF)}) + tas_{(AREF)}, \tag{1}$$

where $tas_{(AAAB)}$ is the output Arctic annual absolute temperature, $tas_{(GAB)}$ is the global absolute temperature, $tas_{(GREF)}$ is the average 1850-1900 global absolute temperature and $tas_{(AREF)}$ is the average 1850-1900 Arctic absolute temperature,

$(tas_{(GAB)}$ - $tas_{(GREF)})$ represents the global mean temperature anomaly and ~~β~~ β_{AA} is the regression coefficient representing the Arctic Amplification factor with a range between 2.5 and 4 about a median of 3, and is derived from the linear regression between the global mean and Arctic annual mean temperature anomaly. To generate the absolute temperature $(tas_{(AAAB)})$, the 1850-1900 mean Arctic absolute temperature $(tas_{(AREF)})$ for ~~the first ensemble member of~~ each CMIP6 model was added to the Arctic annual mean temperature anomaly (~~$\beta \cdot (tas_{(GAB)} - tas_{(GREF)})$~~ $\beta_{AA} \cdot (tas_{(GAB)} - tas_{(GREF)})$), to produce CMIP6 absolute temperatures.

4.2.1 Observational Constraint on Arctic Amplification

Given the disparity between simulated and observed Arctic Amplification trends, a more complex approach is required to constrain model trends to align with observational data. We note that due to the poor signal to noise ratio, we require warming to reach $0.45°C$ over a 20-year period before deriving Arctic Amplification from the observational record. As such, we focus our analysis on Arctic Amplification trends from 1970. The resultant parameterisation of our constraint on Arctic Amplification is as follows:

$$\text{Arctic Amplification}_{r,p,s} = \frac{p}{(1 + \exp(s \cdot (-r + 0.5)))} \frac{\beta_{\text{constantAA}}}{(1 + \exp(S_{\text{linAA}} \cdot (-r_{\text{magicc}} + 0.5)))}. \tag{2}$$

Equation (2) is a sigmoid that initially assumes a linear increase of Arctic Amplification with global mean temperature at a rate dictated by ~~s~~ S_{linAA}, which progresses asymptotically towards a constant Arctic Amplification prescribed by the parameter ~~p~~ $\beta_{\text{constantAA}}$, after which the amplification factor will remain constant as warming continues. ~~r represents~~ $\beta_{\text{constantAA}}$ represents randomly sampled values from the calibrated CMIP6 Arctic Amplification range (β_{AA}) in Eq. 1, while S_{linAA} represents randomly sampled values from the Arctic Amplification observational range (we provide further details in Supplementary Sect. A1). r_{magicc} represents a randomly sampled MAGICC global mean temperature ensemble member, while its negative sign (~~$-r$~~ $-r_{\text{magicc}}$) indicates that the sigmoid should increase rather than decrease with warming. We add a fixed factor of 0.5 to the exponential term to control the temperature at which the Arctic Amplification begins to increase, as the observed Arctic Amplification rises from a mean of approximately 1 as warming grades rise above $0.45°C$ (fig. 3). The division of ~~p~~ $\beta_{\text{constantAA}}$ with the non-linear exponential term ~~on~~ in the denominator, ~~$(1 + \exp(s(-r) + 0.5))$~~ $(1 + \exp(S_{\text{linAA}}(-r_{\text{magicc}}) + 0.5))$, controls the sigmoidal increase of Arctic Amplification with global warming at a rate prescribed by observations, while remaining constant thereafter to account for the modelled CMIP6 trend~~(see Supplementary Sect. A1).~~.

6

4.3 Step ii: The Arctic Seasonal Temperature Parameterisation

We develop our seasonal temperature parameterisation to reflect three 'key features' of warming on the evolution of the seasonal temperature cycle. The first is the asymmetric warming between summer and winter which gradually reduces the amplitude of the seasonal temperature cycle over the calibration period (fig. 4), (Bintanja and Linden, 2013; Zhang et al., 2021; Screen et al., 2012). Secondly, the pre-industrial period (1850-1900) seasonal temperature cycle is relatively symmetrical as the rate of warming from winter to summer is similar in magnitude to the rate of cooling back to winter. However, as the Arctic warms and sea ice declines, the temperature cycle widens at its peak as the melt season lengthens and warm summer temperatures persist into the autumn months. Finally, we find the temperature amplification is not linear in all months. From the mid-21st century the temperature amplification increases during the summer months (June-August), declines in autumn and early winter (September-January), and remains relatively constant through late winter and spring (February-April) (Supplementary fig. A2). The likely cause of the seasonal amplification difference is outlined by Dai et al. (2019), and is related to the seasonal exchange of fluxes between the ocean surface and atmosphere, which respond differently to variations in the rate of sea ice loss to rising CO_2 emissions. We represent these trends via a nested, exponential cosine function that emulates the shape of the seasonal temperature curve in each year, and is controlled by the Arctic annual mean temperature:

$$P = f F_{amp} \cdot \left(\cos(m \cdot g G_{waveLen} - e E_{pShift} \cdot \exp\left(\cos(m^a)\right) \exp\left(\cos(m^{A_{meltLen}})\right)\right)), \tag{3a}$$

$$tas_{(AMAB)} = P(1 + h_{vertShift}), \tag{3b}$$

where ~~$tas_{(AAAB)}$ is the Arctic annual~~ $tas_{(AMAB)}$ is the seasonal Arctic mean temperature in degrees Celsius emulated in step i, m is an equally spaced value between 0 and 2π representing the average point of each month of the year (0 and 2π represent January of year t and January of year $t+1$ respectively) and ~~f, g, and a~~ F_{amp}, $G_{waveLen}$, and $A_{meltLen}$ are model-specific calibration parameters dependent on the Arctic annual mean temperature. ~~f~~ F_{amp} represents the amplitude, ~~g~~ $G_{waveLen}$ controls the wavelength, while ~~a~~ $A_{meltLen}$ (Eq. 3c) is a simple cosine function that controls the change from a basic cosine curve to a shallow, linear temperature decline, as warmer summer temperatures gradually pervade into September, October, November and December (Supplementary fig. A3). ~~e~~ E_{pShift} is a non-temperature dependent and non-model specific parameter with a value of 0.3, that fixes the phase shift of the curve and therefore controls the rate of change from summer to winter temperatures. Finally, ~~h~~ $h_{vertShift}$ (Eq. 3d) is a non-optimised ~~parameter that moves the temperature curve vertically~~, dimensionless function that modulates 'P' by offsetting the temperature to ensure the emulated Arctic annual mean temperature input at time t is equal to the mean of the parameterised monthly temperature curve and is calculated at every time step. ~~f and g~~ F_{amp} and $G_{waveLen}$ are calculated from the calibration coefficients f_1, f_2, g_1 and g_2 that are optimised through a series of simple linear

~~regression~~ regressions dependent on the Arctic annual mean temperature; (~~f~~ F_{amp} = $(f_1 \cdot tas_{(AAAB)}) + f_2$) and ~~g~~ $(G_{\text{waveLen}}$ = $(g_1 \cdot tas_{(AAAB)}) + g_2)$, Supplementary table. A2~~).~~ We acknowledge that while ~~f and g~~ F_{amp} and G_{waveLen} are related, the complexity of the system did not allow us to find a functional form to capture their relationship. As such, we handle these two parameters separately.

$$\tag{3c} \underline{a}\,A_{\text{meltLen}} = \cos((tas_{(AAAB)} \cdot -a_1) - a_2) + a_3,$$

$$\tag{3d} h_{\text{vertShift}} = \frac{tas_{(AAAB)} - \overline{P}}{f}\,\frac{tas_{(AAAB)} - \overline{P}}{F_{\text{amp}}}.$$

The first key feature (see above) is encapsulated by parameter ~~f~~ F_{amp}, which reduces the amplitude of the curve with warming. The second is satisfied by the exponent of the cosine ~~$\exp(\cos(m^a))$~~ $\exp(\cos(m^{A_{\text{meltLen}}}))$. This feature lengthens the summer season as the Arctic annual mean temperature increases. Although our function initially assumes a basic cosine curve at lower values of $tas_{(AAAB)}$, this feature creates the increasingly asymmetric and broad peaked curve as $tas_{(AAAB)}$ rises, generating a left skewed curve at higher Arctic annual mean temperatures. Finally, adding the exponent into the nested cosine (~~$\cos(m(\cos(m^a)))$~~ $\cos(m(\cos(m^{A_{\text{meltLen}}})))$) prevents the temperature in the autumn months rising as fast as the winter months, reducing the amplification from the mid-21st century while simultaneously increasing the amplification during summer. The combined decline in amplitude (~~f~~ F_{amp}) and increase in wavelength (~~g~~ G_{waveLen}) prevents the increase in summer amplification initially, however as the wavelength increases the curve becomes more left skewed causing the rate of July and August warming to increase. This satisfies the third key feature of the seasonal temperature evolution we identify in CMIP6 models.

Analysis of the few models with runs to 2300 (CanESM5), show the shape of the temperature curve doesn't evolve significantly past 2100. As such, we cap the evolution of our calibration parameters to ensure they remain constant past an Arctic annual mean temperature of 6°C (Supplementary fig. A4). Past this temperature, ~~h~~ $h_{\text{vertShift}}$ (Eq. 3d) is the only parameter that continues to change. We find the temperature parameterisation produces a plausible timeseries to 2300 using this method (Supplementary fig. A5).

4.3.1 Bias Corrections to Arctic Monthly Temperature Parameterisation

CMIP6 projections of the mean 1979-2020 Arctic summer (April-July) temperatures are on average ~~warmer~~ 2°C warmer than observed (Supplementary fig. A6). To overcome this, we apply a constant offset to our CMIP6 calibrated temperature in each month, which ~~is~~ we define as the difference between the 1979-2020 mean from observations and that of our emulation. We

acknowledge the 1979-2020 period is a short time frame and internal variability could be a large factor causing this difference. However, as future observations become available and the impact of internal variability is better understood, this bias correction can be updated in future versions of ~~our emulator~~the SASIE framework.

CMIP6 models also project a weaker summer (July and August) warming trend than is observed (Supplementary fig. A6). Simulated July and August temperatures increase slowly from 1980 to 2050 before rising significantly thereafter, whereas observed temperatures rise rapidly from ~1980. We address this by forcing the calibration parameter '~~f~~F_{amp}', which represents the amplitude of the temperature curve in each year in Eq. (3b), to remain constant until the annual mean Arctic temperature reaches an absolute level of -8°C. Our bias correction ensures the summer temperatures increase at the observed rate, while protecting our emulation of the lengthening melt season (Serreze and Barry, 2011).

4.4 Step iii: The SIA Parameterisation

We parameterise the response of Arctic sea ice area to the seasonal Arctic warming trend, as this is ultimately the temperature sea ice responds to (as opposed to global-average warming itself). As CMIP6 models reproduce the observed Arctic warming trend well, this method also ensures our SIA projections respond to Arctic warming trends that match the observed, reducing the number of bias corrections in stage 2.

4.4.1 The Seasonal Melt and Growth Weighting Scheme

The response of Arctic sea ice to temperature is impacted by many different physical processes such as snow cover and ocean heat content changes. Variations in sea ice thickness in particular ~~offers~~ offer insight into how the different rate of ice area growth and melt can be incorporated into our ~~emulator~~framework. During autumn freeze-up, a thin layer of sea ice will rapidly form over the Arctic Ocean. However, during the melt season, a greater thickness of ice needs to melt before the SIA is greatly affected. This produces a differing inertia to temperature changes between the growth and melt of SIA, where for a given temperature change the loss or gain of SIA will be greater in autumn compared to that of spring (Ritschel, 2024; Eisenman, 2010). We therefore apply a weighting scheme to the emulated temperature that forces our SIA parameterisation, to account for the inertia in the sea ice system (Supplementary fig. A7). The updated temperature ('tas') therefore becomes a product of the current month, $tas_{(m)}$ and the previous month, and is computed via the following weighting scheme:

$$tas_{(new)} = \frac{(tas_{(m)} \cdot w_1) + (tas_{(m-1)} \cdot w_2)}{w_1 + w_2} \frac{(tas_{(m)} \cdot w) + (tas_{(m-1)} \cdot 1 - w)}{w + 1 - w},$$

(4a)

where $tas_{(m)}$ is the Arctic temperature at the monthly timestep m, $tas_{(m-1)}$ is the temperature from the previous month and w and $1-w$ are the weightings applied to the current and previous month respectively.

When applying a greater weight to the previous month's temperature in spring, the updated temperature is colder as a greater weight is placed on the colder winter temperatures (Supplementary fig. A7b). Spring SIA is therefore forced with a colder temperature to express the slower decline of SIA for a given temperature change through the melt season. Whereas, the updated temperature is higher in autumn as it becomes a function of the the previous warm summer month, to capture the faster growth of sea ice for an equivalent temperature change through the growth season.

Due to the effect of 'geographic muting' described in Sect. 1, Arctic summer sea ice declines linearly with Arctic warming while the loss of winter sea ice accelerates with warming as the ice pack detaches from land (Ritschel, 2024). Given these characteristics, we develop the following parameterisation to reflect the sigmoidal decline of SIA with Arctic warming:

$$\mathrm{SIA} = \frac{(\mathrm{SIA_{max}} + d) \cdot (1 + \exp(tas_{(t=0)} - b)) - a(tas - tas_{(t=0)})}{(1 + \exp(tas - b))} \frac{(\mathrm{SIA_{max}} + d_{\mathrm{offset}}) \cdot S_{\mathrm{fix}} - L_{\mathrm{linSIA}}(tas - tas_{(t=0)})}{(1 + \exp(tas - b_{\mathrm{nonlinSIA}}))}, \qquad (4b)$$

$$S_{\mathrm{fix}} = (1 + \exp(tas_{(t=0)} - b_{\mathrm{nonlinSIA}})), \qquad (4c)$$

where $\mathrm{SIA_{max}}$ (Eq. 4d) is the seasonal SIA in 1850 and is optimised for each model, ~~a, b and d~~ L_{linSIA}, $b_{\mathrm{nonlinSIA}}$ and d_{offset} are model dependent calibration factors and 'tas' is the weighted Arctic seasonal temperature emulated in step ii.

The resultant functional form initially assumes a slow linear decline of SIA with temperature, which progresses asymptotically towards a constant SIA of 0 million km^2 at higher temperatures (fig. 5). Our SIA parameterisation is therefore derived from the division of a linear and non-linear ('tas') term. The linear response term on the numerator ~~$a(tas - tas_{t=0})$~~ $L_{\mathrm{linSIA}}(tas - tas_{t=0})$ controls the initial linear decline of SIA with temperature and is scaled via the subtraction of the 'tas' in 1850 from subsequent 'tas' in each year; while the exponential 'tas' term ~~$(1 + \exp(tas - b))$~~ $(1 + \exp(tas - b_{\mathrm{nonlinSIA}}))$ on the denominator, controls the sigmoidal decline of SIA and therefore the increase in the sensitivity of sea ice loss to warming in the colder months. The starting term ~~$(\mathrm{SIA_{max}} + d) \cdot (1 + \exp(tas_{(t=0)} - b))$~~ $(\mathrm{SIA_{max}} + d_{\mathrm{offset}}) \cdot S_{\mathrm{fix}}$ fixes the initial SIA in each month, and is the maximum SIA susceptible to melting. $\mathrm{SIA_{max}}$ is ~~vertically shifted via d~~ offset via d_{offset} to account for the chaotic nature of pre-industrial sea ice fluctuations for small warming grades, and the imperfect nature of emulations. An exponential 'tas' term is added for the timestep 0 to account for the increase in the exponent of 'tas' as the initial temperature nears 0°C in the summer months, ensuring that the maximum SIA is equal to $\mathrm{SIA_{max}}$+~~d~~ d_{offset} in the summer months. The CMIP6 seasonal cycle of SIA in 1850 contains a few key features that justify the more complex adapted sine function in Eq. (4d) (Supplementary fig. A8) below:

$$SIA_{max} = f A_{amp} \cdot (-\exp\left(\sin(m^g \cdot a - e)\right)\exp\left(\sin(m^{C_{crest}} \cdot W_{waveLen} - K_{pShift})\right)) + d V_{verShift}, \tag{4d}$$

$$e K_{pshift} = (a W_{waveLen} \cdot 0.8003) + 1.5016, \tag{4e}$$

where m is again an equally spaced value between 0 and 2π representing the average point of each month of the year (0 and 2π represent January of year t and January of year $t+1$ respectively). Calibration factors ~~a, f and d~~ $W_{waveLen}$, A_{amp} and $V_{vertShift}$ control the wavelength, amplitude and vertical shift respectively. The parameter ~~e~~ K_{pshift} controls the phase shift and is a constant derived from a linear regression of ~~a~~ $w_{waveLen}$. The exponent of the sine ~~$-\exp(\sin(m^g))$~~ $-\exp(\sin(m^{C_{crest}}))$ is added to flatten the trough of the curve, as August and September have similar pre-industrial values. Whereas the ~~m^g~~ $m^{C_{crest}}$ term modulates the roundness of the peaks, to ensure the SIA increases sharply from January to its peak in March. This term allows the wavelength to capture the slow transition from winter SIA to summer SIA, while capturing the faster transition from summer SIA to winter SIA in 1850. Finally, we use a negative exponent to represent the decline in SIA through the summer months. The parameter ~~e~~ K_{pshift} then adds a small phase shift to adjust the phase to each specific model. The SIA_{max} factor is first optimised and then input into the SIA calibration.

4.4.2 Bias Corrections to the Sea Ice Area Parameterisation

Similarly to the Arctic seasonal temperature bias correction, we find the modelled 1979-2014 mean SIA between June and September is on average 1.14 million km^2 smaller than observations suggest (fig. A6). To address this, we adjust SIA_{max} in each month by subtracting the difference between the 1979-2020 mean observed SIA and our emulated mean.

We also find that applying the bias-corrected temperature from Sect. 4.3.1 to our SIA parameterisation generates a much larger sea ice loss per degree of warming than is indicated by both CMIP6 models and observations (Supplementary fig. A9). This is to be expected as our corrected temperatures rise at a faster rate between 1979 and 2050 than in CMIP6 projections, while our calibrations representing the response of SIA to Arctic warming remain unchanged. This causes the sensitivity of SIA loss to increase at a cooler temperature, as the sensitivity parameter '~~b~~ $b_{nonlinSIA}$' (Eq. 4b), is reached much earlier than in our calibration. To overcome this, we adjust '~~b~~ $b_{nonlinSIA}$' by subtracting the difference in the mean 1979-2050 Arctic temperature produced from bias correcting the calibration parameter '~~f~~ F_{amp}', and the CMIP6 calibrated temperature where the calibration parameter '~~f~~ F_{amp}' has not been bias corrected. This approach forces the sensitivity to increase at the calibrated temperature and year that CMIP6 models suggest, while also allowing the temperatures to rise at the same rate as observations. The impact of this difference is minimal in the colder months but more pronounced in the summer, as '~~b~~ $b_{nonlinSIA}$' tends to be reached before 2050 through the summer months while it is ~~reach~~ reached much later in winter.

11

5 Results

5.1 ~~Assessing~~ Evaluating the CMIP6 Framework's Performance ~~of our Emulator to 2300~~ in Capturing Rapid Ice Loss

Through this section, we evaluate the ability of our CMIP6 ~~emulator~~ calibrated parameterisations to reproduce the CMIP6 response of SIA to warming in each month when extended to 2300, with particular focus on its ability to project the rapid dis-appearance of March sea ice. This approach aligns with our aim to emulate long-term winter sea ice loss using only information available within the 19th, 20th and 21st centuries. This provides insight into the framework's potential to emulate winter sea ice in models that lack projections beyond 2100. While multiple evaluation strategies are possible, we focus on this method as it directly tests the long-term generalisability of our parameterisation framework. Two additional evaluation approaches are provided in the Supplementary information (fig. A11 and fig. A12) to provide an evaluation of our framework on a non-calibrated scenario and ensemble member. However here, we focus on the performance of long-term sea ice reproduction. We note that ~~when referring to our~~ our use of the term '2100 calibration' ~~we refer~~ refers to our calibration between 1850 and 2100, while our 'out of sample' test refers to ~~emulator output when we force our 2100 calibrations~~ output produced by forcing this calibration with extended global warming projections to 2300.

We find our 2100 calibrations hold 'out of sample', projecting an ice-loss between 1850 and 2300 that aligns with the CMIP6 trend for each month and model, successfully capturing the rapid loss of March sea ice to both global and Arctic warming (fig. 6 and Supplementary fig. B1). We evaluate the goodness of fit (GOF) between our emulation of SIA to 2300 with the corresponding CMIP6 model ~~using a weighted residual sum of squares~~ via the root mean squared error (RMSE), ~~divided~~ dividing by the number of calibrated model years. The GOF statistics of the March sensitivity to Arctic warming show an RMSE ~~correlation~~ of 0.0037 and a correlation coefficient of 0.99, while the fit against global warming produces a RMSE ~~fit~~ of 0.07. Both statistics suggest the successful performance of our ~~emulator~~ parameterisations to 2300. We propose the slightly weaker fit to global warming is because this relationship carries the uncertainties from all three steps of our ~~emulator~~ framework, while the relationship to Arctic warming only carries the uncertainties from one step. While the GOF statistics suggest a successful fit in most months, May in IPSL-CM6A-LR shows a slightly weaker fit (fig. 6). While our weighting scheme accounts for the lag in the response of sea ice to temperature between the growth and melt seasons, May technically requires a larger weight (w) than the growth months. However, our parameterisation only uses a single weight across all SSPs and timescales (1850–2100) to reduce the number of free parameters, missing this variation. Despite a weaker melt-season fit, it remains sufficient for emulation.

Our results suggest that our calibration to 2100 is sufficient to project the non-linearity of winter sea ice loss, however, the majority of models analysed indicate that rapid March ice loss occurs after 2100. We attribute this ability of our ~~emulator~~ parameterisations to project the rapid March ice loss, despite it occurring outside the calibration range of our data, to the combination of the sigmoidal nature of our SIA parameterisation (Eq. 4b), which inherently assumes the rate of ice loss will increase once the threshold temperature controlled by '$b_{nonlinSIA}$' is reached, and the temperature weighting scheme (Eq. 4a).

12

Although March generally does not warm enough to cause an increase in the rate of ice loss before 2100, the early winter and melt season months (November, December and May), show an increase in the sensitivity before 2100. While the specific temperature 'threshold' at which the sensitivity increases at varies between the months and models, it is our calibration of the sensitivity in the early winter and melt season months that informs ice loss after 2100.

The Arctic temperature at which rapid ice loss occurs is relatively similar in November and December, whereas the threshold temperature in May is much warmer (Supplementary fig. A7). We attribute this to the different paces in growth and melt of Arctic sea ice, discussed in Sect. 4.4.1, suggesting the temperature threshold at which the ice pack detaches from land, causing rapid ice loss, will be cooler in the growth season than in the melt season (Ritschel, 2024). Our temperature weighting scheme presented in Sect. 4.4.1, (Eq. 4a), parameterises this difference which subsequently updates the threshold temperature of rapid ice loss. Without the weighting scheme, the sigmoidal nature of our parameterisation would cause the SIA to decline at the same temperature in each month, at the value set by the sensitivity parameter '$\bcancel{b}b_{\text{nonlinSIA}}$' (Supplementary fig. A7a). By calibrating to the rapid ice loss in the early growth (November and December) and melt season (May) months that exhibit rapid ice loss before 2100, our calibration scheme understands the different temperature required to melt and grow ice in both seasons and generates a single value for the weight and sensitivity parameters (w and $\bcancel{b}b_{\text{nonlinSIA}}$) to capture the seasonal cycle in each model. Our SIA parameterisation then assumes that w and $\bcancel{b}b_{\text{nonlinSIA}}$ will have the same effect on the months that don't exhibit rapid ice loss before 2100 as the months that do over the calibrated period.

Through this section, we have evaluated the performance of the SASIEv.1 framework by assessing its ability to capture the abrupt loss of winter sea ice, outside of the calibration period. Two additional evaluation approaches are also provided in the Supplementary information (fig. A11. Here, we first applied the calibration parameters from the first ensemble member of each emulation model to the non-calibrated scenario SSP4-6.0, to consider the out-of-sample performance. We additionally applied these parameters to the full suite of ensemble members from a test case model, CanESM5. We find our parameterisations reproduce SSP4-6.0 and the majority of ensemble members tested well, indicating that our approach provides a good approximation of the ensemble range and can be applied to scenarios beyond those calibrated. While a large aim of framework development involved capturing the rapid loss of winter sea ice, the framework is also designed for broader application. Future work could explore its performance across a wider range of experiments, such as overshoot pathways where we expect our SIA parameterisation to respond to temperature recovery, as seen in SSP1-2.6 (Supplementary Fig. S14). Assessing its ability to emulate experiments beyond the temporal and structural assumptions of the calibrated ESMs would be valuable for future framework application.

5.2 Reproducing the Observed Sensitivity

Here we ~~assess~~ evaluate whether the constraints we apply to our ~~emulator~~ parameterisations in stage 2, are sufficient to capture the observed sensitivity of sea ice loss to global warming. To do so, we compare our emulator to the 'plausible' range defined by the SIMIP Community (2020), which accounts for both the structural and internal variability, by taking two standard deviations

355 of the multi-model CMIP6 ensemble as the uncertainty range around the observed sensitivity of sea ice loss between 1979 and 2014. We take the sensitivity as the regression coefficient between the global temperature and SIA projections over the period 1979-2014 (fig. 7). Although our emulator generates projections in all months, we focus on the September sensitivity as CMIP6 models tend to underestimate the summer sensitivity while reproducing the winter trends relatively well.

When we constrain our ~~emulator~~ parameterisations to address both the 'hot model' problem and the Arctic Amplification bias~~in~~
360 ~~our emulator~~, we project a sensitivity ~~than~~ that matches the 'plausible' range relatively well in most months. In September, our ~~emulator~~ framework projects that a median of -4.06 million km^2 of sea ice is lost per degree of warming between 1979 and 2014, aligning with the 'plausible' September sensitivity of -3.95 million $km^2/°C$ relatively well. Similarly, when assessing how well our projections aligns with the 'plausible' amount of sea ice loss per metric ton of emitted CO_2, we find our observationally constrained emulator projects a sensitivity of -2.5 ~~m~~$\pm$ $0.95 m^2$/~~t~~tCO_2, which falls within the 'plausible' estimate of -2.73 $\pm$
365 $1.37 m^2$/~~t~~tCO_2. While our interquartile range is slightly larger than the 'plausible' against global warming~~is slightly larger~~, and slightly smaller than the 'plausible' against CO_2 emissions, this is expected due to the probabilistic nature of our ~~emulator~~ framework constraints and the influence of model uncertainty from CMIP6 multi-model calibration.

5.3 Application: What is the Temperature and Remaining Carbon Budget Necessary to Prevent Arctic Sea Ice Loss Crossing Critical Thresholds?

370 Through the previous sections we have evidenced that our ~~emulator~~ SASIEv.1 parameterisation framework can reproduce observed sensitivity trends, while also successfully extending projections to 2300. ~~This allows us to apply our emulator to answer key questions in~~ Here we apply the framework to understand the impact of its constraints and extension on key questions within the sea ice discourse. We separate our analysis into two regimes; a linear and non-linear regime. The linear decline of sea ice with cumulative CO_2 ~~emissions~~ emissions- measured from 1850- in July through to December, which we define as
375 the linear regime, provides the basis for the calculation of a finite remaining carbon budget, alongside ~~and~~ an assessment of our current progress towards IPCC warming targets. In a second step, we analyse the non-linear ice loss exhibited in extended projections between January and June, which we define as the non-linear regime, to pinpoint the temperature and CO_2 emission threshold at which winter sea ice detaches from land (Supplementary fig. B3). While previous studies have assessed the global mean temperature threshold at which rapid winter ice loss occurs, to the best of our knowledge this is the first study to pinpoint
380 the CO_2 emission at which this occurs, over a much wider ensemble range than previously possible.

5.4 Linear Regime

When translating the constrained sensitivity from ~~our emulator~~ the emulation framework into the remaining carbon budget, we estimate that there is a 50% chance Arctic September sea ice will be lost for an additional 380 ~~Gt~~ Gigatonnes (Gt) of CO_2 emissions from 2024 (fig. 8) (IQR: $-14 GtCO_2$ and $940\,GtCO_2$). Our estimate is smaller than CMIP6 projections, which suggest

a median of 821GtCO$_2$ (IQR: 500GtCO$_2$ and 1220GtCO$_2$) will cause a seasonally ice-free Arctic Ocean. If we assume the average current emission trends of 38Gt of CO$_2$ per year will continue into the future (Lamboll et al., 2023), our updated limit of 380GtCO$_2$ will be reached within the next decade.

Our analysis indicates that, at the lower bound, we have surpassed the remaining carbon budget by ~~14Gt~~ -14Gt of CO$_2$, implying that sufficient carbon has already been emitted to cause a seasonally ice-free Arctic Ocean. However, observational data suggests this is an overestimate as the Arctic Ocean has not yet exhibited seasonally ice-free conditions. We attribute the overestimate to the broader range of our emulator's 2024 SIA projections compared to the more constrained observed values. Although our emulator considers the full range of observed data, its range is larger than the observed as the 2024 SIA shows very little variation across the available observational datasets. This variance likely arises because our ~~model~~ framework is calibrated to the 1850–2100 period over the CMIP6 multi-model range, rather than specifically to the year 2024. Calculating the remaining carbon budget using the same sensitivity and the lower bound of our projected 2024 SIA will produce a smaller budget than the same sensitivity applied to a larger 2024 observed SIA value. This could explain why the lower limit of our ~~emulator~~ emulated range overestimates the carbon budget although the sensitivities align. If we had calibrated our ~~emulator~~ parameterisations to match the observed SIA in September 2023 (3.8 million km^2), our sensitivity range would suggest a remaining 235GtCO$_2$ - 1737GtCO$_2$ could be emitted before ice-free conditions occur.

~~Assessing~~ Further assessment our carbon budgets against IPCC warming targets ~~reveals~~ reveal that the median remaining carbon budget to prevent an ice-free Arctic Ocean in September is larger than the budget for limiting global warming to 1.5°C (275 GtCO$_2$), yet smaller than the budget limiting warming to 2°C (1150 GtCO$_2$) (fig. 9) (Friedlingstein et al., 2023; Lamboll et al., 2023). Under a high and medium emission scenario (SSP5-8.5 and SSP2-4.5), our emulator framework projects SIA will *likely* (IPCC likelihood scale defined in ~~the Supplementary material,~~ Sect. A1) become ice-free at 1.9°C, whereas only 38% of ensembles project an ice-free Arctic Ocean in September at 1.5°C. Interestingly, the probability of an ice-free ocean under a low emission scenario (SSP1-2.6) significantly increases when constraining the sensitivity. Although the probability does not become *likely* by the IPCC definition of 66%, the probability peaks at 59% in 2068 before declining as SIA recovers (fig. 9).

5.5 Non-linear Regime

Our ~~emulator~~ SASIEv.1 framework suggests that March sea ice declines slowly with CO$_2$ initially, at a rate of -0.75m^2/~~t~~ tCO$_2$ (IQR: -0.6 to -0.91m^2/~~t~~tCO$_2$) per emitted ton of CO$_2$ up to a threshold emission of approximately 10,~~000GtCO~~000 Gigatonnes of CO$_2$ (GtCO$_2$) from 2024 (IQR: 7156GtCO$_2$ to 13,596 GtCO$_2$), after which the sensitivity increases to a rate of -2.2m^2/~~t~~ tCO$_2$ (IQR: -1.75 to -2.93m^2/~~t~~tCO$_2$) (fig. 8). The emission threshold we identify corresponds to a median global mean temperature of 5.42°C (IQR: 4.349°C – 6.62°C) (fig. 9). Once the emission/ temperature threshold is exceeded, the Arctic ice pack will detach from land year-round, increasing the sensitivity at which sea ice is lost to cumulative carbon emissions. After this threshold has been reached the Arctic Ocean opens up rapidly.

While SIA tends to decline with CO_2 emissions at the same rate across all scenarios, rapid ice loss only occurs under the high-emission scenario (SSP5-8.5), while the emission reductions in other scenarios prevent the majority of ensembles reaching the thresholds we identify.

6 Discussion

420 In this study, we present an ~~Arctic sea ice emulator that efficiently generates~~ parameterisation framework that efficiently emulates long-term probabilistic projections of Arctic sea ice that capture current trends and the latest physical understanding of the sea ice system from CMIP6 models. We have demonstrated how our ~~emulator~~ framework uses a comparatively simple set of parameterisations to empirically capture the key features of SIA loss with global warming, compared to the complexity, detailed physics and computational costs of CMIP6 models on which it was trained. Building on this foundation, we show

425 that applying constraints to address the 'hot model' problem and underestimation of Arctic Amplification in CMIP6 models, enables our ~~emulator~~ framework to generate SIA projections that reproduce the 'plausible' (observationally derived) sensitivity well. We highlight that our observational constraint on Arctic Amplification is key to aligning ~~our emulator~~the SASIEv.1 framework's sensitivity with observations, as the sensitivity generated from projections forced by the MAGICC temperature and the CMIP6 calibrated Arctic Amplification do not align with observational data. This suggests that the degree of Arctic

430 amplification in climate models may be key to understanding the future of Arctic sea ice.

Our constrained ~~emulator reduces~~ parameterisations reduce the remaining carbon budget to prevent a seasonally ice-free Arctic Ocean from CMIP6 estimates by 441GtCO$_2$ from 2024 at its median. This suggests that limiting global warming to 1.5°C (275 GtCO$_2$) is sufficient to prevent a seasonally ice-free Arctic Ocean, whereas 2°C (1150 GtCO$_2$) proves insufficient. These findings indicate greater emission reductions may be required than current policy solutions suggest. While earlier studies

435 have constrained the timing of an ice-free ocean, most recalibrate the modelled Arctic sea ice output, linearly extrapolate observations to ice-free conditions, or select climate models based on their ability to reproduce the observed rate of sea ice loss (Winton, 2011; Niederdrenk and Notz, 2018; Wang et al., 2021; Sigmond et al., 2018; Kim et al., 2023; Jahn et al., 2024; Poltronieri et al., 2022). These methods conclude that ice-free conditions in September are *likely* at 1.8°C with a range between 1.3°C and 2.9°C of global warming (9). Our results agree well with these approaches projecting a *likely* ocean at 1.89°C.

440 Another crucial insight has been the ability of our ~~emulator~~ emulation framework to capture the rapid loss of winter sea ice to warming outside of the calibration period, from a more extensive ensemble than CMIP6 models are currently able to achieve. We find there is a 50% chance of sea ice detaching from land in March for the emission of a remaining 10,000GtCO$_2$ from 2024, corresponding to a global mean temperature of 5.42°C (IQR: 3.9°C - 6.3°C). When comparing to previous findings, ~~our emulator identifies~~ we project a threshold that is slightly higher than found by Meccia et al. (2020), who use computationally

445 efficient stochastic physics schemes to project rapid winter sea ice loss will occur at 4 ± 0.35°C of global warming. Whereas our threshold falls within the lower range from Drijfhout et al. (2015), who ~~use~~ used five CMIP5 model simulations (due to

the lack of extended runs past 2100) to suggest the threshold occurs at a global mean temperature ranging between 4.5°C and 8.2°C. Our results add to this body of work by providing a more thorough assessment of winter ice loss backed by a wider range of CMIP6 models and observations, which potentially accounts for the slightly different threshold global temperature

450   from our ~~emulator~~emulation framework, than the two studies discussed here.

While our constraint on Arctic Amplification assumes the ratio will remain constant through the simulation period, some CMIP6 models suggest that the Arctic Amplification will decline as sea ice retreats (Dai et al., 2019; Holland and Landrum, 2021). As the amount of remaining sea ice is usually low or ice-free before it impacts the Arctic Amplification in summer, the feedback mechanism would have minimal influence on our model's projections during this season. Whereas in winter, the

455   rate of sea ice loss after the ice pack detaches from land is so high that changes to the Arctic Amplification past this time have little impact on our SIA projections. While we have shown our constrained Arctic Amplification trend increases the likelihood of an ice-free ocean at lower emission levels compared to CMIP6 estimates, its future is uncertain. It is possible our ~~emulator~~ framework projects a conservative estimate of future Arctic Amplification if current trends continue to persist. If so, the Arctic Ocean could become ice-free earlier than our current projections suggest. ~~In addition, recent studies suggest a~~

460   ~~non-negligable portion of sea ice loss is a result of internal tropical-polar teleconnections, that CMIP6 models and therefore our emulator don't currently capture (Baxter and Ding, 2022; Topál and Ding, 2023). It would be interesting for further work to investigate the contribution of polar-tropical teleconnections to sea ice variability in long-term projections, to determine if this could increase the remaining carbon budget we project will prevent ice-free conditions.~~

7 Conclusions

465   This study has presented a novel method of probabilistic sea ice projection through the development and application of ~~an~~ a parameterisation framework for Arctic sea ice ~~emulator. Our emulator's~~ emulation. Our frameworks ability to efficiently extend future seasonal SIA based on the present sensitivity to global temperatures while also considering the range of knowledge within CMIP6 models, proves its use as a tool to ~~answer prominent questions regarding the future of~~ understand the key gaps in current Arctic sea ice ~~.~~ projections outlined in Sect. 1. This method fills the gap in the literature between complex CMIP6

470   projections, recalibration of model output, and the simple linear extrapolation of sea ice area with anthropogenic forcing. The results from the application of ~~our emulator~~ the SASIEv.1 emulation framework bring into question whether mitigation efforts are stringent enough to prevent critical ice loss, while also providing useful information regarding regime changes in sea ice loss that could cause ice-free conditions to occur rapidly year-round.

Author contributions. SC and MM conceptualised the study. SC conducted data collection, analysis, and validation and served as the primary developer of the framework's parameterisations, with co-development and supervision from MM. SC also performed the model application analyses and prepared the initial manuscript draft, while MM contributed to manuscript review and editing.
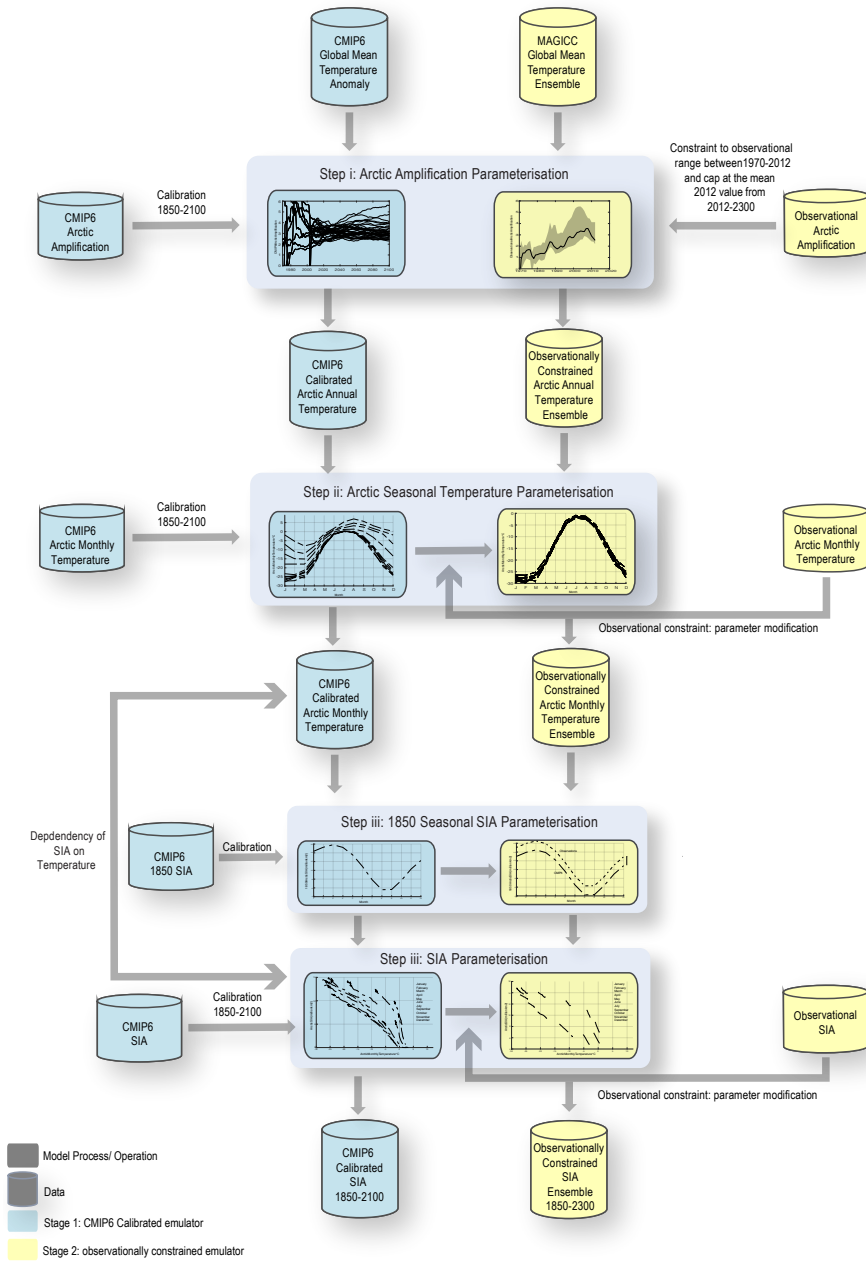
~~Conceptual model~~

Figure 1. A work-flow of ~~emulator development~~the parameterisation framework. Blue cylinders and boxes represent the calibration to CMIP6 models in Stage 1. Yellow cylinders and boxes represent the constraint to observational data in Stage 2. Cylinders represent the data that is used in each parameterisation step, while boxes represent the output from each parameterisation step. Refer to Sections 4.2.1 and 4.2.1 for more information on Step i. Refer to Section 4.3 for more information on Step ii. While section 4.4 provides more information on Step iii.

19
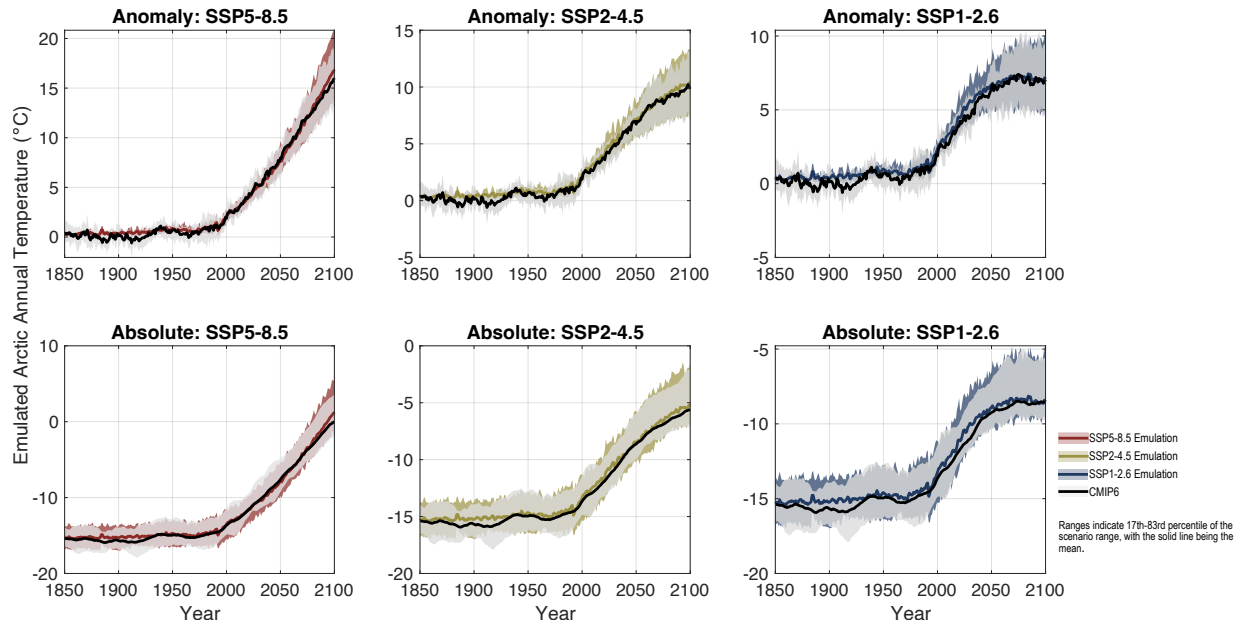
Figure 2. Emulation of CMIP6 calibrated Arctic annual mean temperatures. The top row represents the calibrated temperature anomaly, while the bottom row represents the calibrated absolute temperature. Red, yellow and blue shading represents the *likely* (17th-83rd percentile) calibrated model range for the scenarios SSP5-8.5, SSP2-4.5 and SSP1-2.6 ~~likely (17th-83rd percentile) calibrated range~~, with darker solid lines representing the mean in each scenario. Light grey shading represents the CMIP6 *likely* range and solid black lines represent the CMIP6 multi-model median.
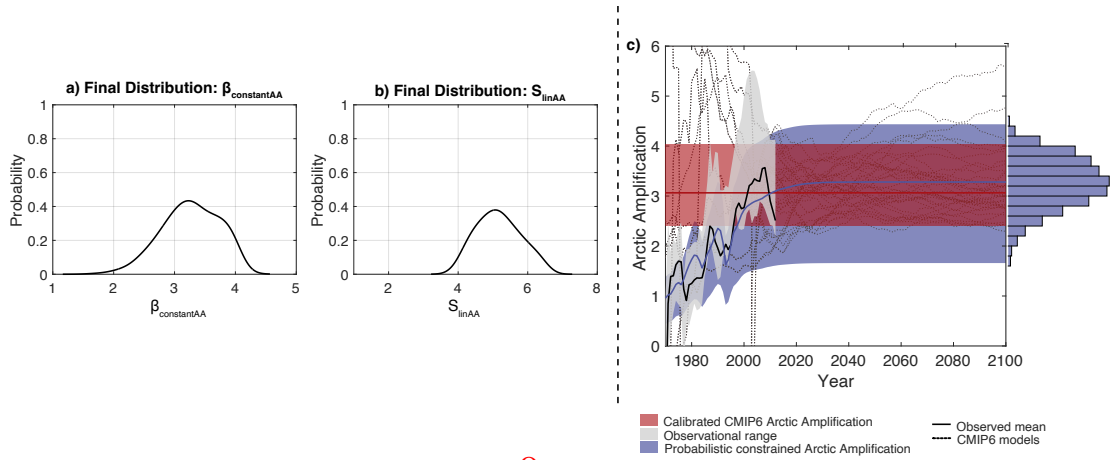
Figure 3. Constrained Arctic ~~amplifications~~ Amplification from our parameterisation framework, as presented in Eq. 2, a and b) represent the probability distributions of $\beta_{constantAA}$ and S_{linAA} respectively, the driving parameters in our constrained Arctic Amplification equation (Eq. 2). c) shows the final constrained Arctic Amplification. Light grey shading represents the *'very likely'* (5th-95th percentile) ~~observational~~ observed Arctic Amplification range, ~~where~~ whereas the black solid line is the observational mean. Red shading represents the *'very likely'* CMIP6 calibrated Arctic Amplification range (Eq. 1), ~~where~~ whereas the red solid line is the CMIP6 calibrated multi-model mean. Blue shading represents the final constrained uncertainty range, while the blue histogram represents the frequency of each Arctic Amplification ~~uncertainty~~ value in the range. We take 2012 as the final year of observations, as it is the last year a central point can be taken with 10 years either side to calculate the 21-year trend without reducing the number of years in the trend, which could bias the trend of the final years.
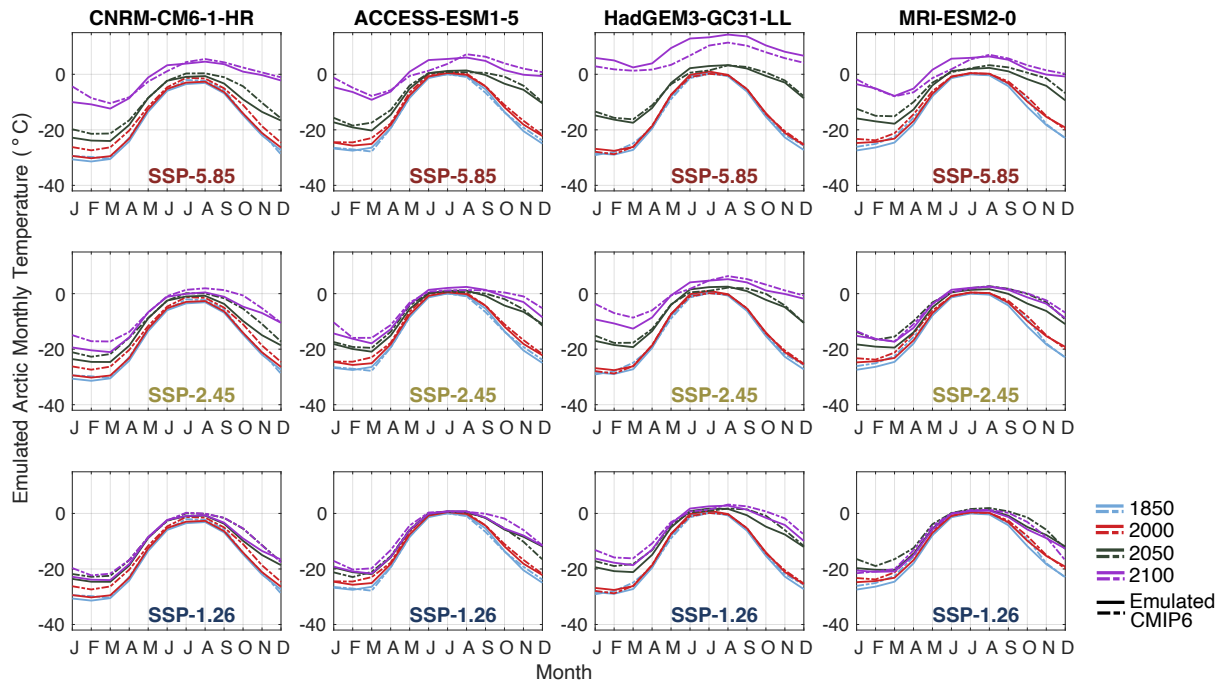
Figure 4. Emulation of the CMIP6 Arctic seasonal temperature cycle in 4 selected years and models. Each column represents our emulation of one model, where the top, middle and bottom rows represent SSP5-8.5, SSP2-4.5 and SSP1-2.6 respectively. Solid lines represent our emulation of a selected CMIP6 model and dashed lines of the same colour represent the CMIP6 data. Only emulation of the years 1850, 2000, 2050 and 2100 are ~~are~~ displayed for visualisation purposes, however calibration was conducted over each year between 1850 and 2100, were one year represents one curve.
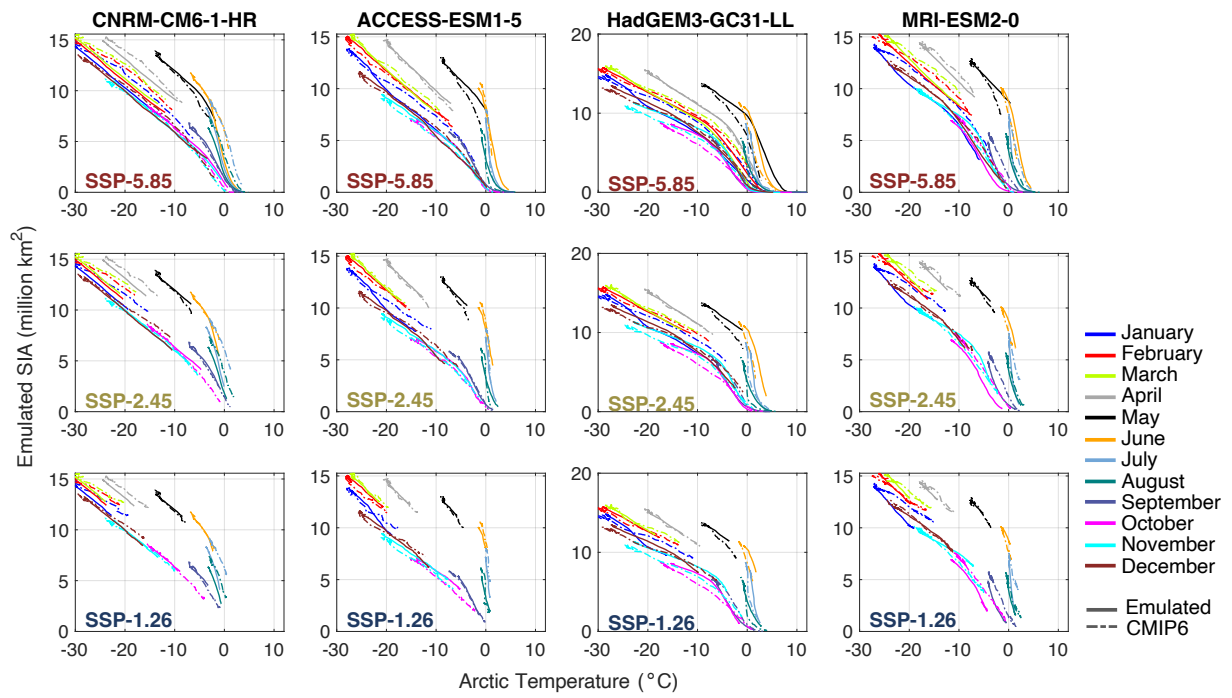
Figure 5. Emulation of the CMIP6 Arctic seasonal Sea Ice Area cycle in 4 selected models. Each column represents our emulation of the SIA under three scenarios from one CMIP6 model, where the top, middle and bottom rows represent SSP5-8.5, SSP2-4.5 and SSP1-2.6 respectively. Solid lines represent our emulation of the CMIP6 SIA in each month, and dashed lines of the same colour represent the CMIP6 data.
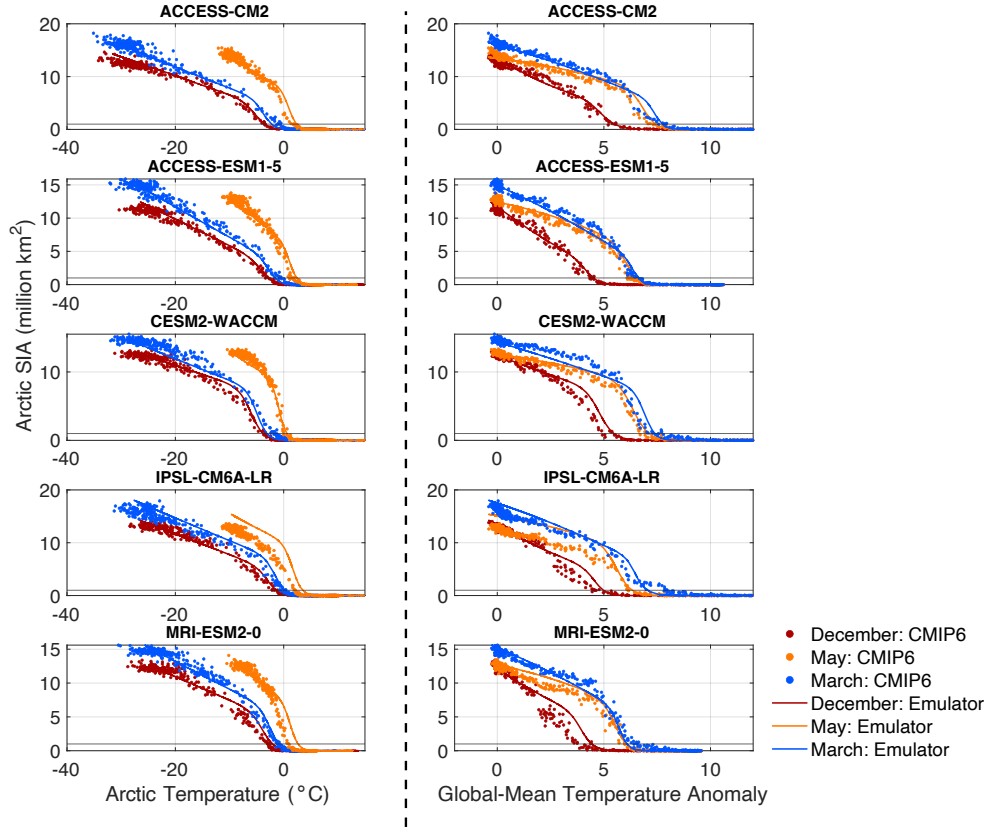
Figure 6. Comparison of the winter sea ice response to Arctic and global warming trends in 'out of sample' extended runs between our ~~emulator~~ emulation framework and CMIP6 data. The left column shows the SIA response to Arctic warming in extended projections between 1850 and 2300, while the right panel shows the SIA response to global warming in extended projections over the same period. Each row represents one of the five CMIP6 models analysed for each warming trend. Solid lines represent our emulation of the CMIP6 response while scatter points represent the CMIP6 model response. We only show three months here for clarity.
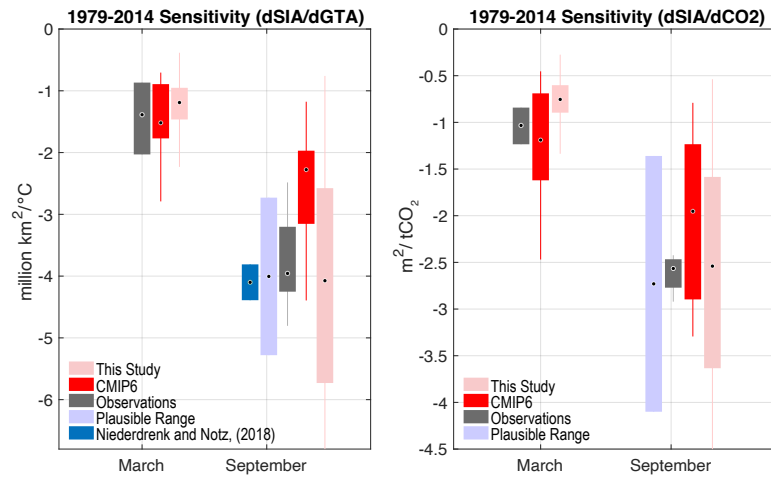
Figure 7. Comparison of the SIA sensitivity to global warming and cumulative CO_2 emissions from 1850 in March and September between our ~~emulator~~framework output, CMIP6 models and observations. For each month, dark red boxplots denote the sensitivity in CMIP6 models, dark grey boxplots denote the sensitivity from observations, light blue boxes represent the 'plausible' range from observations, light pink boxplots show the sensitivity generated from our observationally constrained emulator, dark blue boxes represent the sensitivity from Niederdrenk and Notz, (2018). All boxplots extend from the lower to upper quartile values over the interquartile range, with a point at the median. Whiskers show the full range of values, excluding outliers.
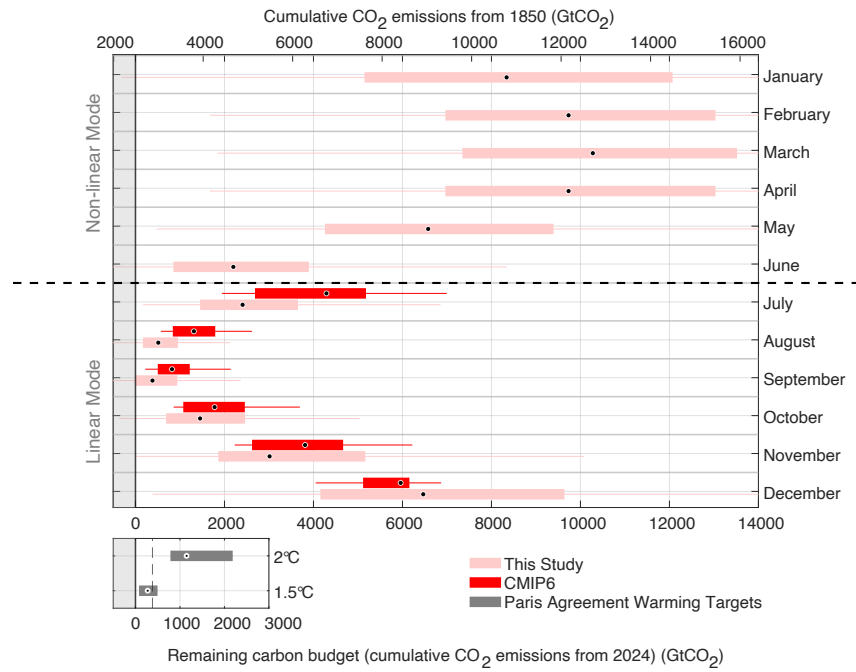
Figure 8. The carbon budget to prevent a seasonally ice-free Arctic Ocean in the linear mode months (July-December) and the carbon budget to prevent rapid ice loss occurring in the non-linear mode months (January-June). Light pink boxplots represent the remaining carbon budgets from 2024, calculated from our emulator. Red boxplots show the remaining carbon budget calculted from the CMIP6 models used in this study. Grey boxplots in the bottom panel compare our results with the remaining carbon budget to prevent Paris Agreement warming targets. The dashed line in the bottom panel compares our emulator's budget for a 50% chance of preventing ice-free conditions in September with the remaining carbon budget to prevent a 1.5°C warming target. Finally, grey vertical shading represents carbon emissions that would exceed the budget to prevent an ice-free ocean or to prevent non-linear ice loss in the winter months. Boxplots represent the interquartile range of the data with the median shown through the black and white dot.
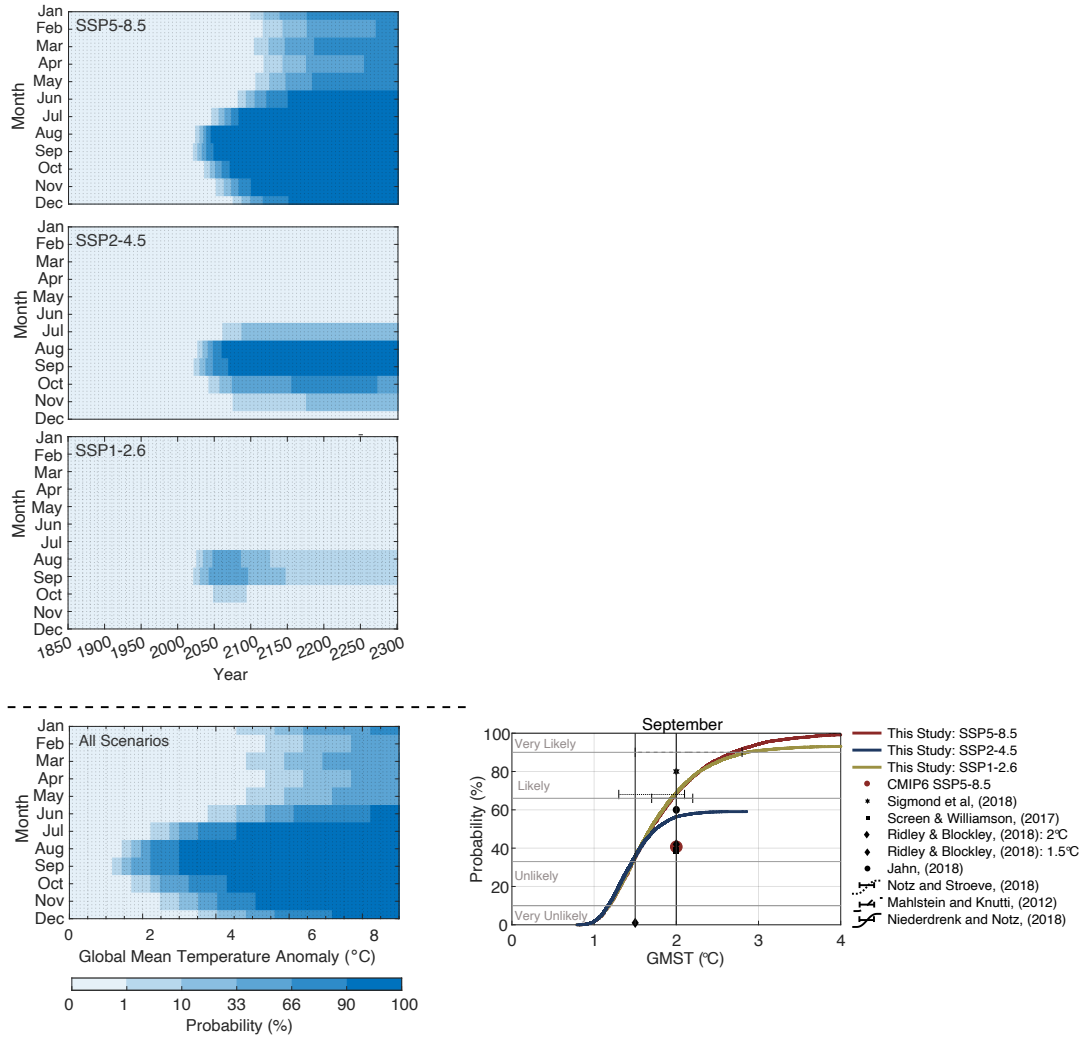
Figure 9. The probability of ice-free conditions in each month, year and global mean temperature by 2300 generated from our observationally constrained ~~emulator~~parameterisations. The probability in each year under SSP5-8.5, SSP2-4.5 and SSP1-2.6 are given in the upper three panels. The probability as a function of global temperature is shown in the bottom panel, and is calculated from the likelihood of ice-free conditions at each global temperature under all three scenarios combined. Darker blue patches represent increasingly ice-free conditions, while whiter patches indicate years and temperatures where a high percentage of emulator ensemble members project high ice cover above 1 million square kilometers. The right panel represents the cumulative probability of the global mean temperature at which the SIA falls below 1 million km^2 for the first time in our observationally constrained ~~emulator~~parameterisations. Red, yellow and blue represent SSP5-8.5, SSP2-4.5 and SSP1-2.6 respectively. Errorbars and scattered shapes represent probability ranges from other studies.

References

Armour, K. C., Eisenman, I., Blanchard-Wrigglesworth, E., McCusker, K. E., and Bitz, C. M.: The reversibility of sea ice loss in a state-of-the-art climate model, Geophysical Research Letters, 38, https://doi.org/10.1029/2011GL048739, 2011.

Balaji, V., Maisonnave, E., Zadeh, N., Lawrence, B. N., Biercamp, J., Fladrich, U., Aloisio, G., Benson, R., Caubel, A., Durachta, J., et al.: CPMIP: measurements of real computational performance of Earth system models in CMIP6, Geoscientific Model Development, 10, 19–34, 2017.

Bathiany, S., Notz, D., Mauritsen, T., Raedel, G., and Brovkin, V.: On the Potential for Abrupt Arctic Winter Sea Ice Loss, Journal of Climate, https://doi.org/10.1175/JCLI-D-15, 2016.

Baxter, I. and Ding, Q.: An optimal atmospheric circulation mode in the Arctic favoring strong Summertime Sea ice melting and ice–albedo feedback, Journal of Climate, 35, 6627–6645, 2022.

Bintanja, R. and Linden, E. C. V. D.: The changing seasonal climate in the Arctic, Scientific Reports, 3, https://doi.org/10.1038/srep01556, 2013.

Bonan, D. B., Lehner, F., and Holland, M. M.: Partitioning uncertainty in projections of Arctic sea ice, Environmental Research Letters, 16, https://doi.org/10.1088/1748-9326/abe0ec, 2021.

Chylek, P., Folland, C., Klett, J. D., Wang, M., Hengartner, N., Lesins, G., and Dubey, M. K.: Annual Mean Arctic Amplification 1970–2020: Observed and Simulated by CMIP6 Climate Models, Geophysical Research Letters, 49, https://doi.org/10.1029/2022GL099371, 2022.

Chylek, P., Folland, C. K., Klett, J. D., Wang, M., Lesins, G., and Dubey, M. K.: High Values of the Arctic Amplification in the Early Decades of the 21st Century: Causes of Discrepancy by CMIP6 Models Between Observation and Simulation, Journal of Geophysical Research: Atmospheres, 128, https://doi.org/10.1029/2023JD039269, 2023.

Dai, A., Luo, D., Song, M., and Liu, J.: Arctic amplification is caused by sea-ice loss under increasing CO2, Nature Communications, 10, https://doi.org/10.1038/s41467-018-07954-9, 2019.

DeRepentigny, P., Jahn, A., Holland, M. M., and Smith, A.: Arctic sea ice in two configurations of the CESM2 during the 20th and 21st centuries, Journal of Geophysical Research: Oceans, 125, e2020JC016 133, 2020.

Doerr, J., Notz, D., and Kern, S.: UHH Sea Ice Area Product, 2021.

Douville: Robust and perfectible constraints on human-induced Arctic amplification, Communications Earth and Environment, 4, https://doi.org/10.1038/s43247-023-00949-5, 2023.

Drijfhout, S., Bathiany, S., Beaulieu, C., Brovkin, V., Claussen, M., Huntingford, C., Scheffer, M., Sgubin, G., and Swingedouw, D.: Catalogue of abrupt shifts in Intergovernmental Panel on Climate Change climate models, Proceedings of the National Academy of Sciences of the United States of America, 112, E5777–E5786, https://doi.org/10.1073/pnas.1511451112, 2015.

Eisenman: Geographic muting of changes in the Arctic sea ice cover, Geophysical Research Letters, 37, https://doi.org/10.1029/2010GL043741, 2010.

Friedlingstein, P., O'Sullivan, M., Jones, M. W., Andrew, R. M., Bakker, D. C., Hauck, J., Landschützer, P., Quéré, C. L., Luijkx, I. T., Peters, G. P., Peters, W., Pongratz, J., Schwingshackl, C., Sitch, S., Canadell, J. G., Ciais, P., Jackson, R. B., Alin, S. R., Anthoni, P., Barbero, L., Bates, N. R., Becker, M., Bellouin, N., Decharme, B., Bopp, L., Brasika, I. B. M., Cadule, P., Chamberlain, M. A., Chandra, N., Chau, T. T. T., Chevallier, F., Chini, L. P., Cronin, M., Dou, X., Enyo, K., Evans, W., Falk, S., Feely, R. A., Feng, L., Ford, D. J., Gasser, T., Ghattas, J., Gkritzalis, T., Grassi, G., Gregor, L., Gruber, N., Özgür Gürses, Harris, I., Hefner, M., Heinke, J., Houghton, R. A., Hurtt, G. C., Iida, Y., Ilyina, T., Jacobson, A. R., Jain, A., Jarníková, T., Jersild, A., Jiang, F., Jin, Z., Joos, F., Kato, E., Keeling, R. F., Kennedy, D.,

Goldewijk, K. K., Knauer, J., Korsbakken, J. I., Körtzinger, A., Lan, X., Lefèvre, N., Li, H., Liu, J., Liu, Z., Ma, L., Marland, G., Mayot, N., McGuire, P. C., McKinley, G. A., Meyer, G., Morgan, E. J., Munro, D. R., Nakaoka, S. I., Niwa, Y., O'Brien, K. M., Olsen, A., Omar, A. M., Ono, T., Paulsen, M., Pierrot, D., Pocock, K., Poulter, B., Powis, C. M., Rehder, G., Resplandy, L., Robertson, E., Rödenbeck, C., Rosan, T. M., Schwinger, J., Séférian, R., Smallman, T. L., Smith, S. M., Sospedra-Alfonso, R., Sun, Q., Sutton, A. J., Sweeney, C., Takao, S., Tans, P. P., Tian, H., Tilbrook, B., Tsujino, H., Tubiello, F., van der Werf, G. R., van Ooijen, E., Wanninkhof, R., Watanabe, M., Wimart-Rousseau, C., Yang, D., Yang, X., Yuan, W., Yue, X., Zaehle, S., Zeng, J., and Zheng, B.: Global Carbon Budget 2023, Earth System Science Data, 15, 5301–5369, https://doi.org/10.5194/essd-15-5301-2023, 2023.

Hankel, C. and Tziperman, E.: The Role of Atmospheric Feedbacks in Abrupt Winter Arctic Sea Ice Loss in Future Warming Scenarios, Journal of Climate, https://doi.org/10.1175/JCLI-D-20, 2021.

Hankel, C. and Tziperman, E.: An approach for projecting the timing of abrupt winter Arctic sea ice loss, Nonlinear Processes in Geophysics, 30, 299–309, https://doi.org/10.5194/npg-30-299-2023, 2023.

Hausfather, Marvel, Schmidt, Nielsen-Gammon, and Zelinka: Climate simulations: recognize the 'hot model' problem Setting the agenda in research, Nature, 26, 2022.

Hay, S., Screen, J., and Catto, J. L.: Steady but model dependent Arctic amplification of the forced temperature response in 21st century CMIP6 projections, Environmental Research: Climate, https://doi.org/10.1088/2752-5295/ad4201, 2024.

Hezel, P. J., Fichefet, T., and Massonnet, F.: Modeled Arctic sea ice evolution through 2300 in CMIP5 extended RCPs, Cryosphere, 8, 1195–1204, https://doi.org/10.5194/tc-8-1195-2014, 2014.

Holland, M. M. and Landrum, L.: The Emergence and Transient Nature of Arctic Amplification in Coupled Climate Models, Frontiers in Earth Science, 9, https://doi.org/10.3389/feart.2021.719024, 2021.

IPCC: Climate Change 2021: The Physical Science Basis. Contribution of Working Group I to the Sixth Assessment Report of the Intergovernmental Panel on Climate Change, vol. In Press, Cambridge University Press, Cambridge, United Kingdom and New York, NY, USA, https://doi.org/10.1017/9781009157896, 2021.

IPCC: Climate Change 2022: Mitigation of Climate Change. Contribution of Working Group III to the Sixth Assessment Report of the Intergovernmental Panel on Climate Change, Cambridge University Press, Cambridge, UK and New York, NY, USA, https://doi.org/10.1017/9781009157926, 2022.

Jahn, A., Holland, M. M., and Kay, J. E.: Projections of an ice-free Arctic Ocean, Nature Reviews Earth and Environment, 5, 164–176, https://doi.org/10.1038/s43017-023-00515-9, 2024.

Kim, Y. H., Min, S. K., Gillett, N. P., Notz, D., and Malinina, E.: Observationally-constrained projections of an ice-free Arctic even under a low emission scenario, Nature Communications, 14, https://doi.org/10.1038/s41467-023-38511-8, 2023.

Lagarias, J. C., Reeds, J. A., Wright, M. H., Wright, P. E., and Optim, S. J.: Convergence Properties of the Nelder-Mean Simplex Method in Low Dimensions, Society for Industrial and Applied Mathematics, 9, 112–147, http://www.siam.org/journals/ojsa.php, 1998.

Lamboll, R. D., Nicholls, Z. R., Smith, C. J., Kikstra, J. S., Byers, E., and Rogelj, J.: Assessing the size and uncertainty of remaining carbon budgets, Nature Climate Change, 13, 1360–1367, https://doi.org/10.1038/s41558-023-01848-5, 2023.

Lenssen, N. J., Schmidt, G. A., Hansen, J. E., Menne, M. J., Persin, A., Ruedy, R., and Zyss, D.: Improvements in the GISTEMP uncertainty model, Journal of Geophysical Research: Atmospheres, 124, 6307–6326, 2019.

Mahlstein, I. and Knutti, R.: September Arctic sea ice predicted to disappear near 2°C global warming above present, Journal of Geophysical Research Atmospheres, 117, https://doi.org/10.1029/2011JD016709, 2012.

Meccia, V. L., Fabiano, F., Davini, P., and Corti, S.: Stochastic Parameterizations and the Climate Response to External Forcing: An Experiment With EC-Earth, Geophysical Research Letters, 47, https://doi.org/10.1029/2019GL085951, 2020.

570   Morice, C. P., Kennedy, J. J., Rayner, N. A., Winn, J., Hogan, E., Killick, R., Dunn, R., Osborn, T., Jones, P., and Simpson, I.: An updated assessment of near-surface temperature change from 1850: The HadCRUT5 data set, Journal of Geophysical Research: Atmospheres, 126, e2019JD032 361, 2021.

Nelder, J. A. and Meadf, R.: A simplex method for function minimization, The Computer Journal, 7, 308–313, http://comjnl.oxfordjournals. org/, 1965.

575   Nicholls, Z., Meinshausen, M., Lewis, J., Gieseke, R., Dommenget, D., Dorheim, K., Fan, C.-S., Fuglestvedt, J., Gasser, T., and Golüke, U.: Reduced Complexity Model Intercomparison Project Phase 1: introduction and evaluation of global-mean temperature response, Geoscientific Model Development, https://doi.org/10.5194/gmd, 2020.

Nicholls, Z., Meinshausen, M., Lewis, J., Corradi, M. R., Dorheim, K., Gasser, T., Gieseke, R., Hope, A. P., Leach, N. J., McBride, L. A., Quilcaille, Y., Rogelj, J., Salawitch, R. J., Samset, B. H., Sandstad, M., Shiklomanov, A., Skeie, R. B., Smith, C. J., Smith, S. J., Su, X.,

580   Tsutsui, J., Vega-Westhoff, B., and Woodard, D. L.: Reduced Complexity Model Intercomparison Project Phase 2: Synthesizing Earth System Knowledge for Probabilistic Climate Projections, Earth's Future, 9, https://doi.org/10.1029/2020EF001900, 2021.

Niederdrenk and Notz: Arctic Sea Ice in a 1.5°C Warmer World, Geophysical Research Letters, 45, 1963–1971, https://doi.org/10.1002/2017GL076159, 2018.

Poltronieri, A., Bochow, N., Aksamit, N. O., Boers, N., Jakobsen, P., and Rypdal, M.: Arctic summer sea ice loss will accelerate in coming

585   decades, Environmental Research Letters, 2022.

Rantanen, Karpechko, Lipponen, Nordling, Hyvärinen, Ruosteenoja, Vihma, and Laaksonen: The Arctic has warmed nearly four times faster than the globe since 1979, Communications Earth and Environment, 3, https://doi.org/10.1038/s43247-022-00498-3, 2022.

Ritschel: A transforming Arctic: Unraveling Climate Change Impacts on Sea Ice Dynamics and Oceanic pCO2, https://orcid.org/ 0000-0001-7464-7075, 2024.

590   Rohde, R. A. and Hausfather, Z.: The Berkeley Earth land/ocean temperature record, Earth System Science Data, 12, 3469–3479, 2020.

Rosenblum and Eisenman: Sea Ice Trends in Climate Models Only Accurate in Runs with Biased Global Warming, Journal of Climate, https://doi.org/10.1175/JCLI-D-16-0455.s1, 2017.

Screen, J. A., Deser, C., and Simmonds, I.: Local and remote controls on observed Arctic warming, Geophysical Research Letters, 39, 2012.

Serreze and Barry: Processes and impacts of Arctic amplification: A research synthesis, Global and Planetary Change, 77, 85–96,

595   https://doi.org/10.1016/j.gloplacha.2011.03.004, 2011.

Serreze and Stroeve: Arctic sea ice trends, variability and implications for seasonal ice forecasting, Philosophical Transactions of the Royal Society A: Mathematical, Physical and Engineering Sciences, 373, https://doi.org/10.1098/rsta.2014.0159, 2015.

Sigmond, M., Fyfe, J. C., and Swart, N. C.: Ice-free Arctic projections under the Paris Agreement, Nature Climate Change, 8, 404–408, https://doi.org/10.1038/s41558-018-0124-y, 2018.

600   SIMIP Community: Arctic Sea Ice in CMIP6, Geophysical Research Letters, 47, https://doi.org/10.1029/2019GL086749, 2020.

Topál, D. and Ding, Q.: Atmospheric circulation-constrained model sensitivity recalibrates Arctic climate projections, Nature Climate Change, 13, 710–718, 2023.

Wang, B., Zhou, X., Ding, Q., and Liu, J.: Increasing confidence in projecting the Arctic ice-free year with emergent constraints, Environmental Research Letters, 16, https://doi.org/10.1088/1748-9326/ac0b17, 2021.

605 Winton, M.: Do climate models underestimate the sensitivity of Northern Hemisphere sea ice cover?, Journal of Climate, 24, 3924–3934, https://doi.org/10.1175/2011JCLI4146.1, 2011.

Zhang, R., Wang, H., Fu, Q., Rasch, P. J., Wu, M., and Maslowski, W.: Understanding the cold season Arctic surface warming trend in recent decades, Geophysical Research Letters, 48, e2021GL094 878, 2021.

Supplementary A: Methods

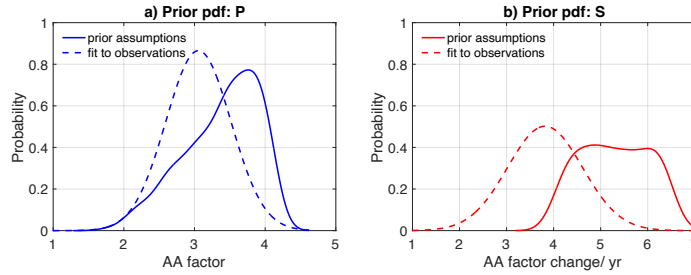### A1 Observational Constraint on Arctic Amplification Supplementary

Figure A1. Contribution of each parameter to the observationally constrained Arctic Amplification between 1970 and 2100. a and b) show the two initial distributions for parameters ~~s~~ S_{linAA} and ~~p~~ $\beta_{\text{constantAA}}$ before they are averaged and normalised. The solid line reflects our assumptions of current and future Arctic Amplification, while the dashed line reflects actual trends from both observations and CMIP6 models.

We generate values for ~~s and p~~ S_{linAA} and $\beta_{\text{constantAA}}$ by averaging two distributions for each parameter (fig. A1a-b). The Bayesian nature of our approach allows us to inform our routine with expert judgement, the first distribution is generated from our assumptions of future and current Arctic Amplification trends. Whereas the second is informed from observational and CMIP6 data. This approach considers CMIP6 data and observations while accounting for the uncertain future of Arctic Amplification due to model biases. For ~~p~~ $\beta_{\text{constantAA}}$ we first generate a right skewed poisson distribution that applies a greater weight to higher Arctic Amplification possibilities, as it is plausible that Arctic Amplification will continue to increase into the future given observed trends (Rantanen et al. (2022); Chylek et al. (2022)). The amplification factor is also physically unlikely to be less than one as this would cause the Arctic to warm at a slower rate than the global mean. For ~~s~~ S_{linAA}, we generate a uniform distribution, as the observational datasets used in this analysis suggest that the rate of increase in Arctic Amplification per degree of warming is generally uniformly spread across its range. The second distribution describes the probability of ~~s and p~~ S_{linAA} and $\beta_{\text{constantAA}}$ based on available observational and model data. For ~~p~~ $\beta_{\text{constantAA}}$, we generate a Gaussian distribution from the standard deviation and mean of the average 2012-2100 CMIP6 Arctic Amplification. Similarly, we set up the second distribution for ~~s~~ S_{linAA} by generating a Gaussian distribution from the mean and standard deviation of the observed rate of Arctic Amplification increase with global warming. We then average and normalise the two distributions for each parameter to generate a single distribution (fig. 3c-d). Our resultant ~~p~~ $\beta_{\text{constantAA}}$ distribution follows a right skewed distribution with a broad peak ranging between 3.5 and 3.8. Whereas our ~~s~~ S_{linAA} distribution is a simple normal distribution about 4.8. This process aims to derive a more realistic description of the key features of Arctic Amplification evolution through distributions informed from observations, models and our best understanding of future trends. We randomly sample values from the final distributions of ~~s, p and r~~ S_{linAA}, $\beta_{\text{constantAA}}$ and r_{magicc} and input these values into Eq. (2), to generate the constrained range of probabilistic Arctic Amplification projections shown in figure 3.

To generate the Arctic annual temperature anomaly, we multiply 'rT_{magicc}' with a randomly sampled Arctic Amplification ensemble member. To convert the anomalies into absolute temperatures, we add the mean 1850-1900 observed absolute Arctic annual temperature to our emulated anomaly projections. We iteratively repeat this process to generate a 600-ensemble member Arctic annual mean temperature ensemble, which is input into our seasonal temperature parameterisation in the next step (step

635   ii).

A2   Additional Figures: CMIP6 Calibration
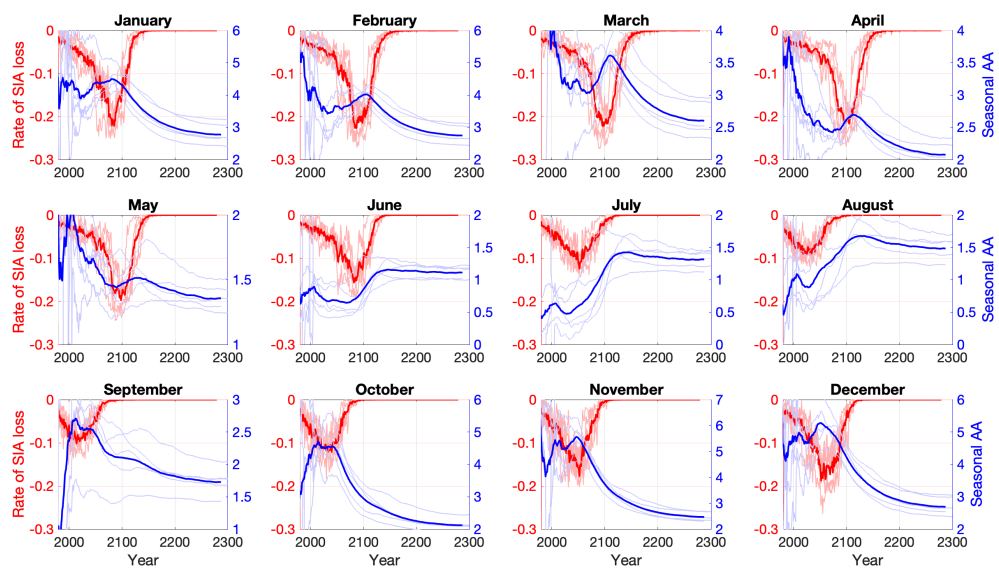
Figure A2. Comparison of the seasonal Arctic Amplification with the rate of SIA loss to 2300. Dark red lines show the mean rate of sea ice loss in each month per year, while lighter red lines show the rate from each of the 5 models used in this analysis. The rate is calculated here as the difference in SIA between each year for each month. Dark blue lines show the mean Arctic Amplification evolution to 2300 in each month, while lighter blue lines show the temperature amplification in each model. The seasonal Arctic Amplification is calculated from the division of the seasonal Arctic temperature by the global mean temperature.
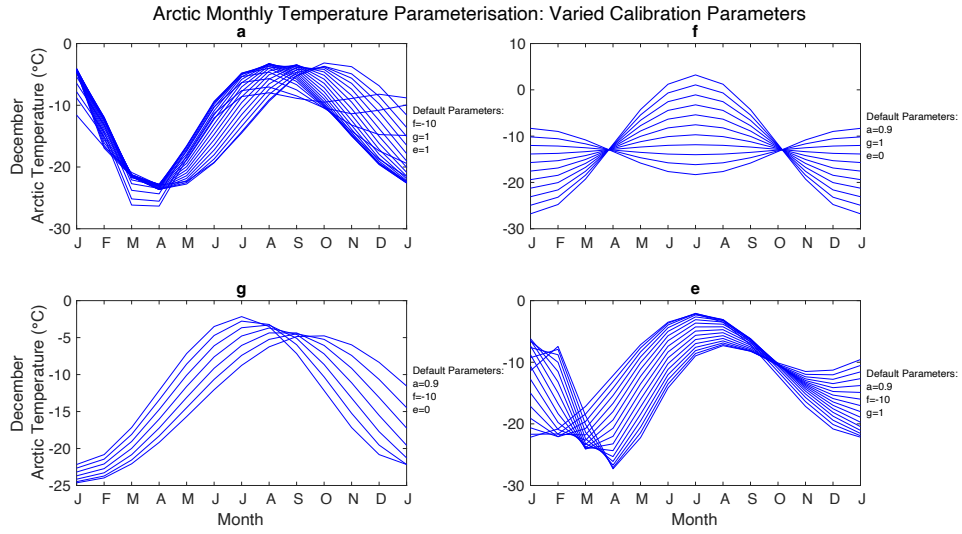
Figure A3. Visualisation of the role of each calibration parameter in our seasonal Arctic temperature parameterisation (Eq. 3b). Each box denotes the evolution of each calibration parameter in our seasonal temperature parameterisation, and how they change with annual temperature. All other parameters in each parameterisation are kept at default values while the parameter of note is varied with temperature.
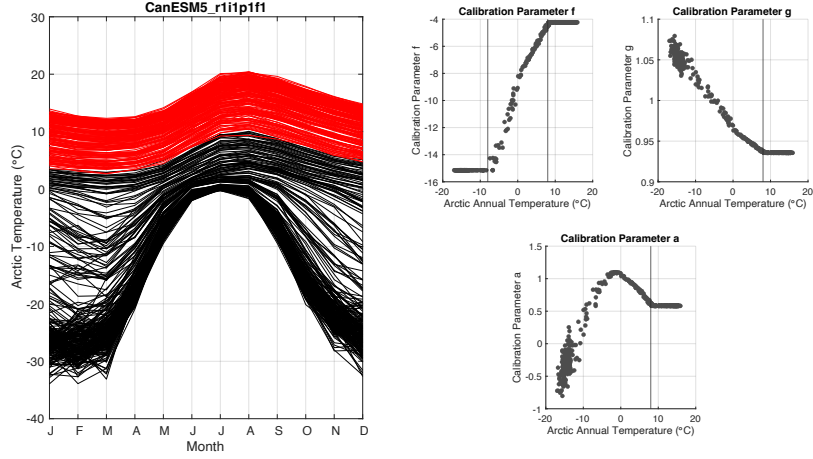
Figure A4. CMIP6 Arctic seasonal temperature cycle 1850-2300. Black lines indicate the 1850-2100 period, while red lines indicate the 2100-2300 period, highlighting the lack of change in shape of the Arctic seasonal temperature cycle after 2100. Box a-c show the temperature dependence of calibration parameters F_{amp}, $G_{waveLen}$ and $A_{meltLen}$, where grey vertical lines indicate the lack of change in these parameters after the Arctic annual temperature reaches 6°C, where they are forced to remain constant with changes to the Arctic annual temperature to prevent further change to the emulated seasonal cycle. The second grey vertical line in the calibration parameter 'F_{amp}' box indicates the Arctic annual temperature 'F_{amp}' is forced to remain constant until to allow summer temperatures to increase at a similar rate to the observed.
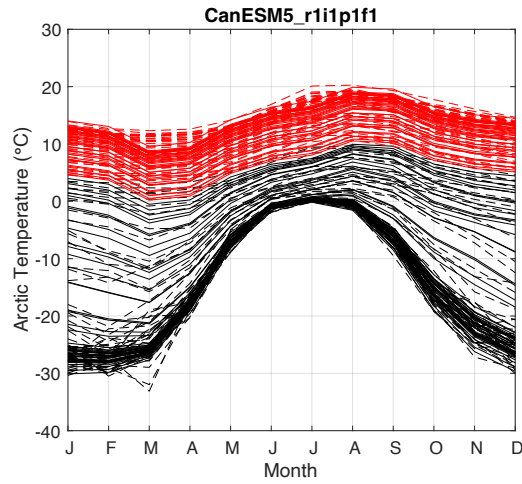
Figure A5. Comparison of our emulated seasonal Arctic temperature evolution with its CMIP6 counterpart to 2300. Black lines represent the 1850-2100 temperature cycle, while red lines represent the 2100-2300 seasonal cycle temperature evolution. Solid lines represent our emulation of the CMIP6 trend, while dashed lines represent CMIP6 data for the first ensemble member of model CanESM5.

35
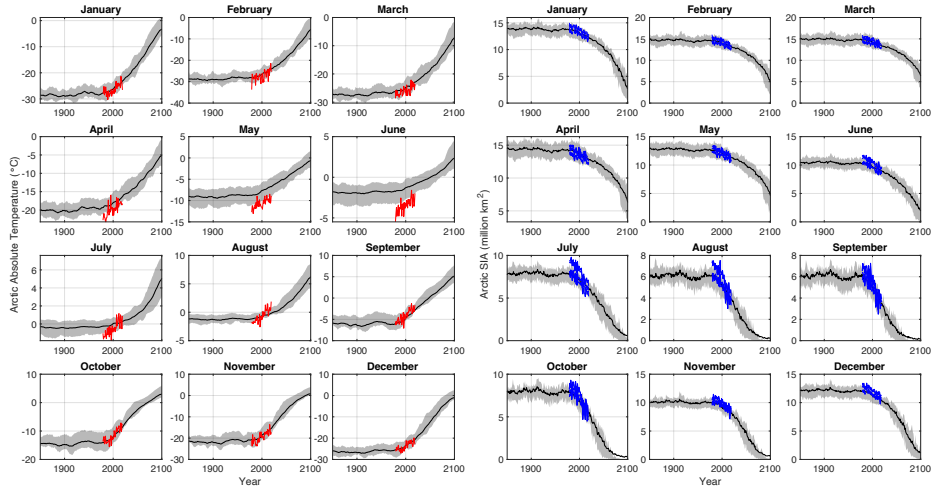
Figure A6. Timeseries of the mean 1979-2014 summer Arctic temperature and SIA bias between CMIP6 models and observations. Shading represents the CMIP6 17th-83rd (*likely*) percentile range, while black lines represent the mean. Left) Arctic monthly surface temperature, observations in red. Right) SIA observations in blue.
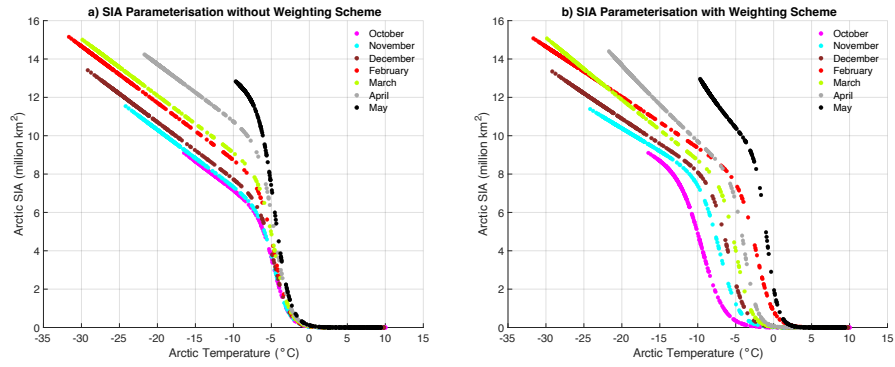
Figure A7. Effect of the weighting scheme on our SIA parameterisation. a) Projections of SIA loss with Arctic warming between October and May without a weighting scheme applied to our SIA parameterisation. b) Projections from the same model as a) when the weighting scheme has been applied. We highlight the warmer temperature of rapid sea ice loss in the melt season than in the growth season.
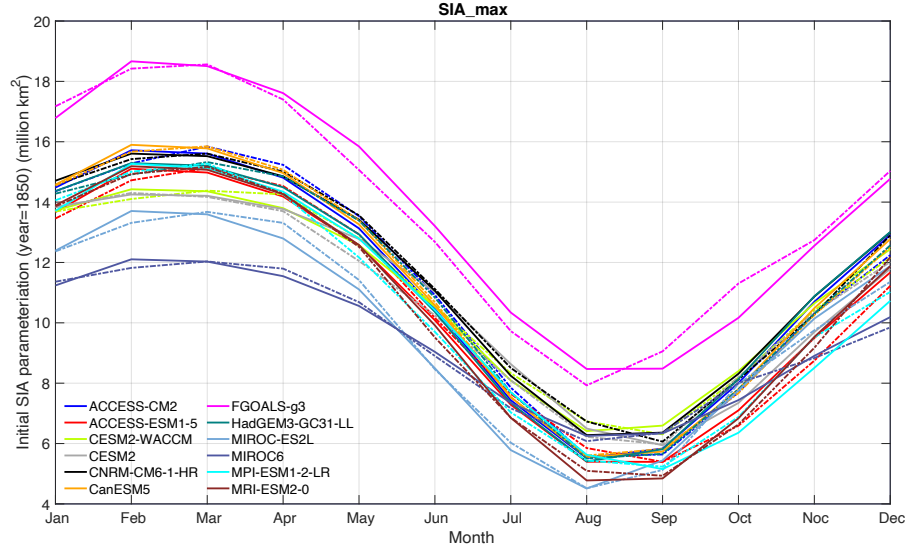
Figure A8. Comparison of our CMIP6 calibrated starting SIA parameter (SIA$_{\overline{max}\,\text{max}}$, Eq: 4d) with its CMIP6 counterpart. Dashed lines represent our calibrated SIA in each month while solid lines represent their CMIP6 counterpart. Each colour represents each of the 12 CMIP6 models used in this study.
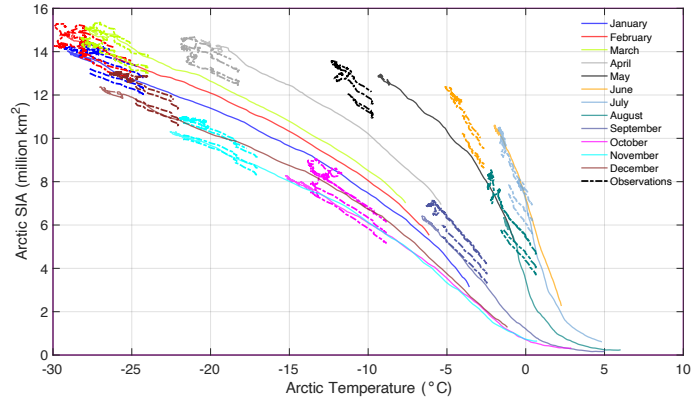
Figure A9. Comparison of the mean CMIP6 SIA as a function of the mean CMIP6 Arctic warming in each month with observations. Showing the higher sensitivity of SIA loss to summer Arctic warming in CMIP6 models than observations. Solid lines represent the CMIP6 mean data in each month and dotted lines represent observations.
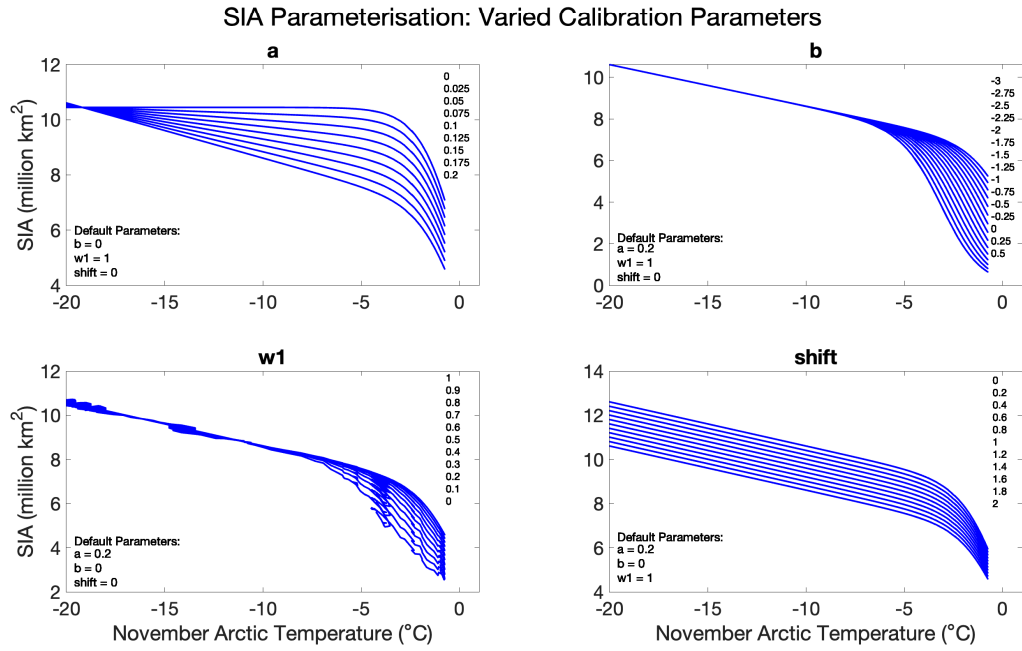
Figure A10. Visualisation of the role of each calibration parameter in our SIA parameterisation (Eq: 5). Each box denotes the evolution of each calibration parameter in our SIA parameterisation, and how they change with temperature. All other parameters in each equation are kept at default values while the parameter of note is varied with temperature.
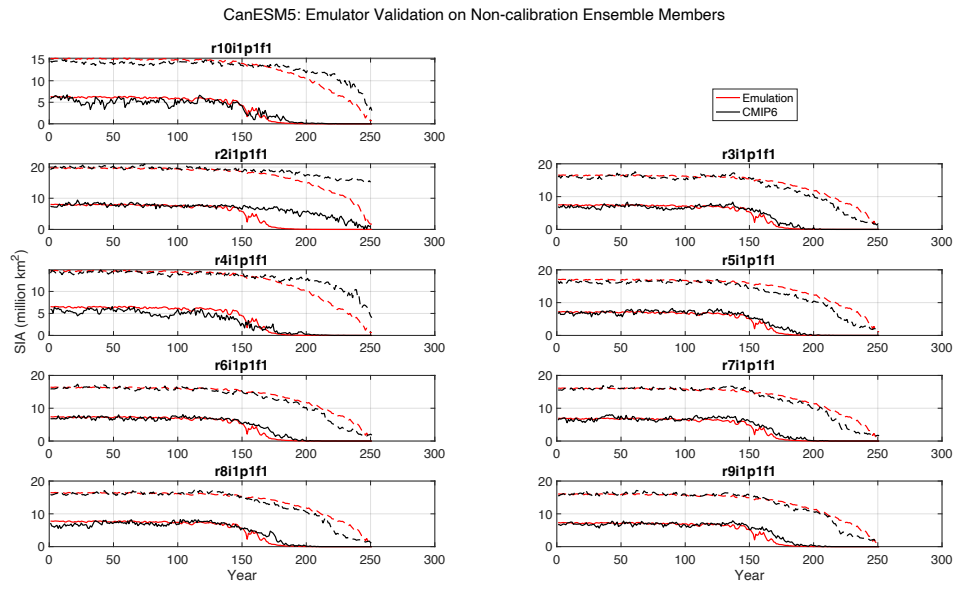
Figure A11. Emulator validation of the CanESM5 on non-calibrated ensemble members. Black dashed lines indicate the CMIP6 ensemble projections, while red dashed lines depict our emulation of each ensemble member.
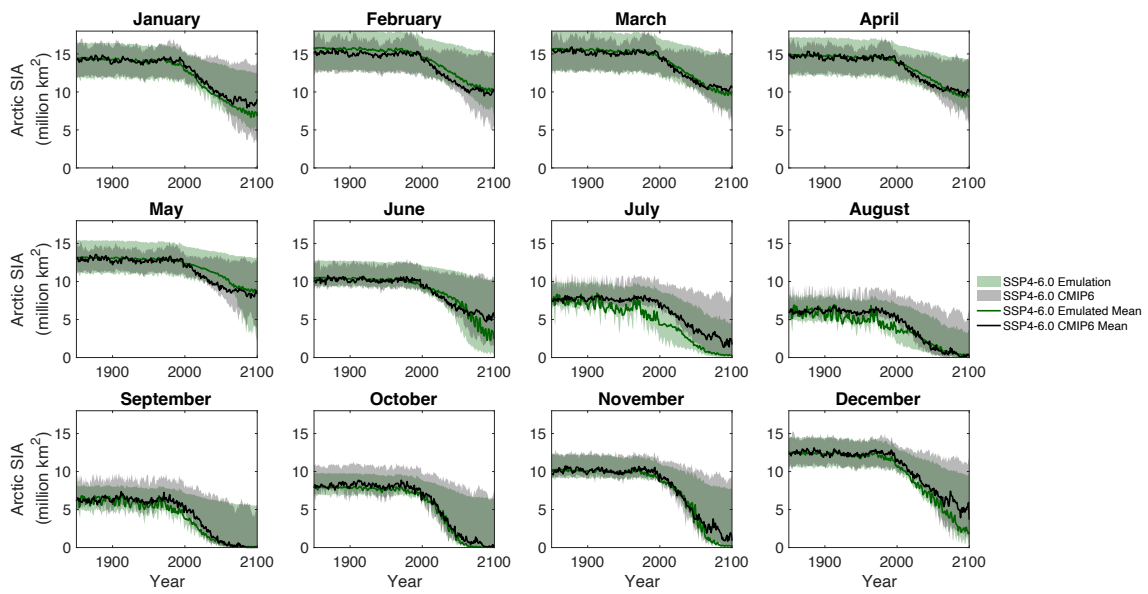
Figure A12. Validation of the emulated structural uncertainty of sea ice loss using the first ensemble member of the uncalibrated SSP4-6.0 scenario. Green shading represents the emulated structural uncertainty of SSP4-6.0, using the parameters generated from our calibration to SSP5-8.5, SSP1-2.6 and SSP2-4.5. Grey shading represents the CMIP6 structural uncertainty of SIA loss for the SSP4-6.0 scenario. Green solid lines represent the emulated SSP4-6.0 mean, while black solid lines indicate the CMIP6 mean projections for the same scenario.

A3 Supplementary Tables

Model Names	*Ensemble*
ACCESS-CM2	r1i1p1f1
ACCESS-ESM1-5	r1i1p1f1
CESM2-WACCM	r1i1p1f1
CESM2	r1i1p1f1
CNRM-CM6-1-HR	r1i1p1f1
CanESM5	r1i1p1f1
FGOALS-g3	r1i1p1f1
HadGEM3-GC31-LL	r1i1p1f1
IPSL-CM6A-LR	r1i1p1f1
MIROC-ES2L	r1i1p1f1
MIROC6	r1i1p1f1
MPI-ESM1-2-LR	r1i1p1f1
MRI-ESM2-0	r1i1p1f1

Table A1. A list of all CMIP6 models and their respective ensembles used during the calibration of our paramterisations, in Sections 4.2, 4.3 and 4.4).

Model Names	$f1$	$f2(^\circ C)$	$g1(C^{-1})$	$g2$	$a1$	$a2$	$a3$
ACCESS-CM2	0.49	-8.43	-0.0063	0.931	-0.07	-0.58	0.10
ACCESS-ESM1-5	0.56	-7.16	-0.0071	0.93	-0.03	0.14	0.13
CESM2-WACCM	0.63	-6.08	-0.0031	0.97	-0.09	-0.63	0.11
CESM2	0.58	-6.29	-0.0042	0.96	-0.09	-0.64	0.11
CNRM-CM6-1-HR	0.42	-7.78	-0.0007	0.97	-0.06	-0.08	0.13
CanESM5	0.54	-7.47	-0.0076	0.95	-0.09	-0.32	0.01
FGOALS-g3	0.35	-11.4	-0.0009	1.03	-0.01	0.64	0.36
HadGEM3-GC31-LL	0.49	-8.33	-0.0062	0.94	-0.09	-0.54	0.07
IPSL-CM6A-LR	0.41	-8.88	-0.008	0.885	-0.044	-0.363	-0.066
MIROC-ES2L	0.45	-9.01	-0.0040	0.98	-0.09	-0.45	0.08
MIROC6	0.44	-8.09	-0.0057	0.95	-0.11	-0.37	0.09
MPI-ESM1-2-LR	0.56	-6.48	-0.0016	0.99	-0.02	0.94	0.57
MRI-ESM2-0	0.52	-7.35	-0.0036	0.96	-0.09	-0.50	0.09

Table A2. Calibration results of the 7 free parameters in the Arctic seasonal parameterisation (step ii, Eq: ~~3b~~3a) ~~calibration results with parameter sets~~ for the available 12 CMIP6 models, given to 3 significant figures. Calibration parameters are introduced in Section 4.3. ~~The mean response of~~ If no units are specified, take the ~~calibration data is given at the bottom of the table~~parameter to be dimensionless.

Model Names	L_{linSIA}	d_{offset}	w	$b_{\text{nonlinSIA}}$	A_{amp}	C_{crest}	W_{waveLen}	K_{pshift}	$V_{\text{vertshift}}$
ACCESS-CM2	0.38	0.39	0.54	-1.32	4.42	0.78	1.51	2.71	17.4
ACCESS-ESM1-5	0.40	-0.04	0.55	-0.98	4.26	0.726	1.62	2.79	16.7
CESM2-WACCM	0.29	0.06	0.21	-4.44	3.49	0.84	1.32	2.56	15.7
CESM2	0.29	-0.13	0.13	-4.43	3.57	0.94	1.05	2.35	15.6
CNRM-CM6-1-HR	0.41	-0.01	1.00	-0.77	4.08	0.82	1.37	2.59	17.1
CanESM5	0.40	0.54	0.55	0.66	4.51	0.76	1.53	2.73	17.6
FGOALS-g3	0.35	-0.14	0.45	0.65	4.46	0.68	1.76	2.91	20.3
HadGEM3-GC31-LL	0.32	0.45	0.27	-0.99	4.28	0.83	1.36	2.59	16.9
IPSL-CM6A-LR	0.36	0.39	0.53	-1.28	4.43	0.69	1.71	2.87	18.5
MIROC-ES2L	0.32	-0.47	0.49	-1.11	3.93	0.76	1.62	2.80	15.2
MIROC6	0.26	0.20	0.00	-1.36	2.55	0.73	1.62	2.80	13.1
MPI-ESM1-2-LR	0.39	-0.44	0.00	-1.71	4.34	0.697	1.66	2.83	16.9
MRI-ESM2-0	0.38	0.09	0.19	-1.83	4.56	0.762	1.52	2.72	16.9
Units	mill Km^2/ $^\circ$C	DimLess	Dimless	$^\circ$C	mill Km^2	Dimless	Dimless	Dimless	mill Km^2

Table A3. Calibration results of the 9 free parameters in the SIA parameterisation (step iii, Eq: 4b) ~~calibration results with parameter sets~~ for the available 12 CMIP6 models, given to 3 significant figures. Calibration parameters are introduced in Section 4.4. ~~The mean response of~~ If no units are specified, take ~~the~~ ~~calibration data~~ the parameter to be dimensionless. 'mill' represents million and DimLess implies the parameter is ~~given at~~ dimensionless, both are shortened to fit all units within ~~the~~ ~~bottom of the~~ the table.

Months	AMST: Standard Deviation		AMST: Mean	
	CE: Emulation	CMIP6	CE: Emulation	CMIP6
January	5.58	5.74	-19.2	-18.5
February	5.51	5.55	-20.4	-20.4
March	4.68	4.88	-20.9	-19.6
April	3.57	3.75	-15.8	-5.08
May	2.43	2.61	-6.50	-4
June	1.65	1.36	-0.48	-0.19
July	1.41	1.02	0.99	0.93
August	1.75	1.77	1.53	1.03
September	2.82	3.18	-0.56	-0.43
October	4.51	5.21	-5.24	-3.67
November	6.25	6.19	-9.04	-8.73
December	7.02	6.28	-13.5	-14.6
Mean	**3.93**	**3.96**	**9.09**	**-8.61**

Table A4. Table of the mean and standard deviation of the average 2080-2100 emulated (CE) Arctic seasonal temperature (AMST) multi-model range in each month. (I extract the 2080-2100 range in model, find the mean in each model, and then calculate the mean and std across all of the models to find the multi-model mean and std). The mean response of the calibration data is given at the bottom of the table. All values are rounded to three significant figures.

Months	SIA: Standard Deviation		SIA: Mean	
	CE: Emulation	CMIP6	CE: Emulation	CMIP6
January	1.83	1.69	9.10	10.8
February	1.78	1.58	11.3	12.1
March	1.68	1.51	12.1	12.4
April	1.49	1.45	11.8	11.9
May	1.26	1.49	10.9	10.3
June	1.52	1.74	8.24	7.77
July	2.09	2.16	3.49	4.36
August	1.89	2.10	2.00	1.99
September	2.09	2.07	1.33	1.51
October	2.34	2.42	2.36	2.76
November	1.75	2.31	5.23	5.57
December	1.83	1.83	7.12	8.77
Mean	**1.79**	**1.86**	**7.09**	**7.53**

Table A5. Table of the mean and standard deviation of the average 2080-2100 emulated (CE) SIA multi-model range in each month. (I extract the 2080-2100 range in model, find the mean in each model, and then calculate the mean and std across all of the models to find the multi-model mean and std). The mean response of the calibration data is given at the bottom of the table. All values are rounded to three significant figures.

Months	SSP5-8.5 SIA: RMSE		SSP2-4.5 SIA: RMSE		SSP1-2.6 SIA: RMSE	
	March	Sept	March	Sept	March	Sept
ACCESS-CM2	0.262	0.288	0.246	0.222	0.249	0.232
ACCESS-ESM1-5	0.0971	0.056	0.085	0.079	0.096	0.097
CESM2-WACCM	0.331	0.430	0.342	0.325	0.360	0.345
CESM2	0.394	0.318	0.629	0.292	0.786	0.229
CNRM-CM6-1-HR	0.193	1.08	0.163	0.970	0.086	1.05
CanESM5	0.253	0.094	0.204	0.196	0.133	0.300
FGOALS-g3	0.395	1.52	0.401	0.697	0.441	0.521
HadGEM3-GC31-LL	0.425	0.201	0.328	0.342	0.273	0.461
IPSL-CM6A-LR	0.236	0.231	0.142	0.342	0.247	0.081
MIROC-ES2L	0.135	0.324	0.134	0.445	0.074	0.467
MIROC6	0.245	0.743	0.306	0.985	0.269	1.24
MPI-ESM1-2-LR	0.218	0.139	0.085	0.215	0.098	0.268
MRI-ESM2-0	0.483	0.176	0.182	0.247	0.082	0.361
Mean	**0.286**	**0.448**	**0.259**	**0.418**	**0.246**	**0.465**

Table A6. Table of the RMSE between the emulated and CMIP6 SIA in each model for March and September. The mean RMSE is given at the bottom of the table. All values are rounded to three significant figures.

Months	SSP5-8.5 SIA: R^2		SSP2-4.5 SIA: R^2		SSP1-2.6 SIA: R^2	
	March	Sept	March	Sept	March	Sept
ACCESS-CM2	0.98	0.97	0.97	0.98	0.94	0.98
ACCESS-ESM1-5	0.98	0.99	0.97	0.99	0.95	0.99
CESM2-WACCM	0.94	0.97	0.93	0.98	0.82	0.98
CESM2	0.94	0.99	0.92	0.99	0.82	0.99
CNRM-CM6-1-HR	0.98	0.91	0.97	0.93	0.97	0.95
CanESM5	0.99	0.99	0.99	0.98	0.98	0.98
FGOALS-g3	0.91	0.98	0.87	0.96	0.74	0.94
HadGEM3-GC31-LL	0.99	0.97	0.99	0.96	0.97	0.95
IPSL-CM6A-LR	0.93	0.98	0.99	0.93	0.97	0.94
MIROC-ES2L	0.99	0.94	0.98	0.91	0.95	0.93
MIROC6	0.97	0.92	0.98	0.89	0.95	0.90
MPI-ESM1-2-LR	0.95	0.98	0.95	0.97	0.95	0.98
MRI-ESM2-0	0.95	0.98	0.95	0.97	0.96	0.97
Mean	**0.96**	**0.96**	**0.95**	**0.96**	**0.92**	**0.96**

Table A7. Table of the R^2 corelation coefficient between the emulated and CMIP6 SIA in each model for March and September. The mean R^2 value is given at the bottom of the table. All values are rounded to two significant figures.

A4 Calculating the Carbon Budget

Here we outline how we calculate the remaining carbon budget in both the linear mode and non-linear mode months. We first focus on the carbon budget to prevent a seasonally ice-free Arctic Ocean in the linear mode months. To quantify the remaining carbon budget in the linear mode months, we simply extract the cumulative CO_2 emission in the first year SIA falls below 1 million km^2. Whereas for those ensembles that do not reach 1 million km^2 by 2300, we interpolate over the linear period to diagnose the cumulative CO_2 emission at 1 million km^2, assuming the linear relationship persists. Additionally, SIA recovers in the low emission scenario (SSP1-2.6) due to its reliance on net negative CO_2 emissions, in particular on BECCS (biomass with carbon sequestration and storage). We therefore do not include ensembles that show SIA recovery in our analysis of the carbon budget in the linear mode months.

We estimate the threshold cumulative CO_2 emissions at which the rapid loss of Arctic sea ice occurs through the non-linear mode months by doubling the value of parameter '$bb_{nonlinSIA}$', as this provides the temperature of rapid SIA loss to Arctic warming. We first double the seasonal Arctic temperature dictated by '$bb_{nonlinSIA}$', then extract the year in which the seasonal Arctic temperature occurs in each non-linear mode month. From this, we then extract the MAGICC cumulative CO_2 emission at the same index, to determine the threshold CO_2 value at which rapid sea ice loss occurs. While the sensitivity of sea ice loss increases after this threshold, the relationship remains linear to ice-free conditions. We therefore calculate the sensitivity over the second linear period as the SIA loss per emitted ton of CO_2 that occurs between the threshold CO_2 emission of rapid ice loss, and the first time each ensemble drops below 1 million km^2. As the cumulative CO_2 emission projections begin in 1750, to analyse the remaining carbon budget from 2024 we simply subtract the cumulative CO_2 emission in 2024 from the total carbon budget in each ensemble.

As the scenarios SSP1-2.6 and SSP2-4.5 show significant emissions reductions, the temperature in the majority of ensembles in both scenarios does not rise significantly enough for sea ice to detach from land causing rapid ice loss. As such, we focus mainly on SSP5-8.5 when pinpointing this threshold. Within this scenario itself, a few ensembles do not reach ice-free conditions by 2300 due to the probabilistic nature of our observationally constrained Arctic Amplification. This is because there is the possibility of randomly sampling a cooler global mean temperature ensemble in combination with a small Arctic Amplification ensemble when calculating the Arctic annual mean temperature. In the ensembles that exhibit rapid ice loss but do not reach ice-free conditions by the simulations end, we estimate the sensitivity by interpolating over the available data. We therefore interpolate the sensitivity after rapid ice loss begins if the SIA continues to decline for at least 10 years after the sensitivity has increased. We therefore assume the constant linear decline of rapid ice loss holds until ice-free conditions occur. We find this to be sufficient as there is little year to year variability in the decline of SIA in our projections. The sensitivity over the 10 years after rapid ice loss begins is therefore also equal to the sensitivity 50 years after it begins.

Supplementary B: ~~Results~~

A1 ~~How Well Does Our CMIP6 Emulator Reproduce CMIP6 Data?~~<u>Calculating the Probability of an Ice-free Arctic Ocean</u>

690 We calculate the likelihood of an ice-free Arctic Ocean occurring in each year as the ratio of the number of ensemble members projecting a SIA of 1 million km^2 or less in each year, to the total number of ensemble members used. Additionally, we calculate the probability of an ice-free ocean occurring at IPCC warming targets via a cumulative distribution function of the global temperature at which sea ice falls below 1 million km^2 for the first time, across the multi-model ensemble. We make use of the IPCC likelihood scale where "*very unlikely*" equates to a probability of 0%–10%, "*unlikely*" equates to 10%–33%, "*as*
695 *likely as not*" equates to 33%–66%, "*likely*" equates to 66%–90%, and "*very likely*" equates to 90%–100%. A 100% probability of an Arctic ice-free ocean is produced when the entire multi-model ensemble projects a SIA below 1 million km^2.

Supplementary B: Results

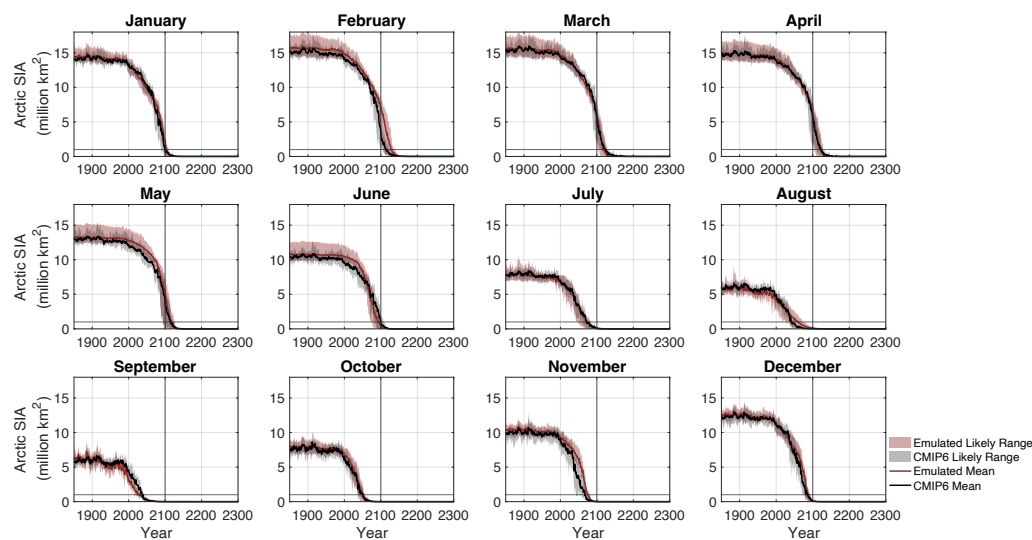### B1 Assessing the Performance of our Emulator to 2300

Figure B1. Emulated seasonal Arctic SIA between 1850-2300. Red shading represents the emulated SSP5-8.5 likely range from our CMIP6 emulator, while grey shading represents the SSP5-8.5 CMIP6 likely range. Red solid lines represent the emulated mean, and solid black line represents the CMIP6 multi-model median.
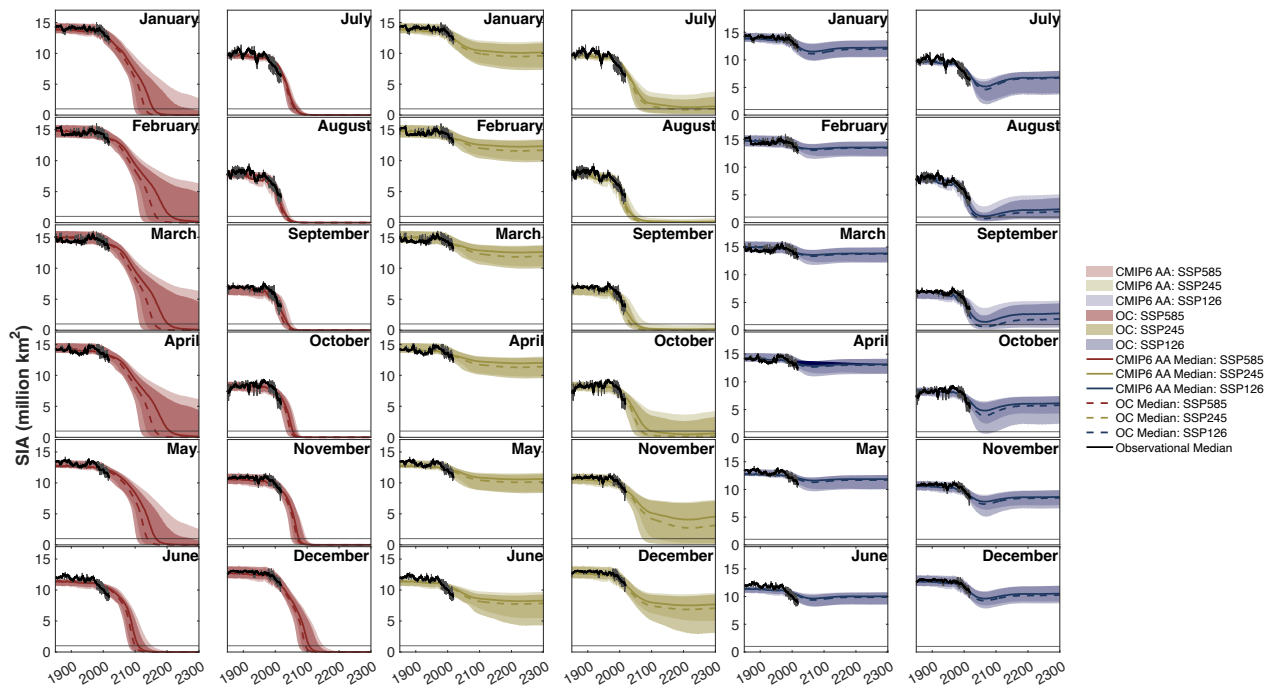
Figure B2. Emulated likely range of the monthly Arctic SIA over the time period 1850-2300 when our emulator is forced with the MAGICC 600-member ensemble global mean temperature anomaly. Red, yellow and blue shading represents SSP5-8.5, SSP2-4.5 and SSP1-2.6 respectively. Darker shading represents the projections from our observationally constrained emulator, and lighter shading represents the projections when forcing our emulator with the CMIP6 calibrated (linear) Arctic Amplification. The dashed and solid lines represent the mean SIA from each set of projections respectively. The black line spanning 1850-2020 represents observational data.
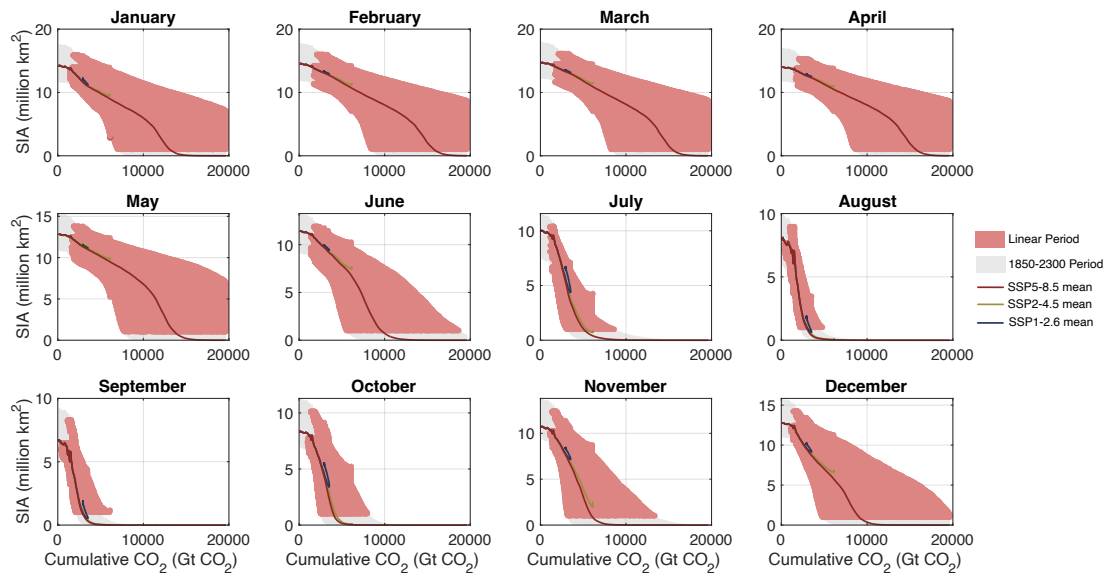
Figure B3. The seasonal decline of Arctic sea ice with cumulative CO_2 emissions. We highlight the difference between linear-mode (July-December) and non-linear mode months (January-June). Light red shading represents the SIA sensitivity to CO_2 emissions over the period between SIA falling below 10% of the pre-indsutrial mean and SIA reaching ice-free conditions ($<$1 million km^2). The 'linear period' is represented through dark red shading, while grey shading represents SIA outside of the 'linear period'. Red, yellow and blue solid lines represent the SSP5-8.5, SSP2-4.5 and SSP1-2.6 mean respectively.

SSPs	March		September	
	Year	GMST(°C)	Year	GMST(°C)
SSP5-8.5	2178	7.7	2037	1.89
SSP2-4.5	N/A	N/A	2046	1.89
SSP1-2.6	N/A	N/A	N/A	N/A

Table B1. Probability of a *likely* ice-free Arctic Ocean in September and March from our OC emulator. N/A implies the probability of an ice-free Arctic Ocean never becomes *likely* in this scenario.

B2 How Well Does Our CMIP6 Emulator Reproduce CMIP6 Data?

700   We test the ability of our emulator to reproduce the CMIP6 Arctic Amplification, Arctic seasonal temperature and SIA response to global warming for the CMIP6 models used in the calibration process.
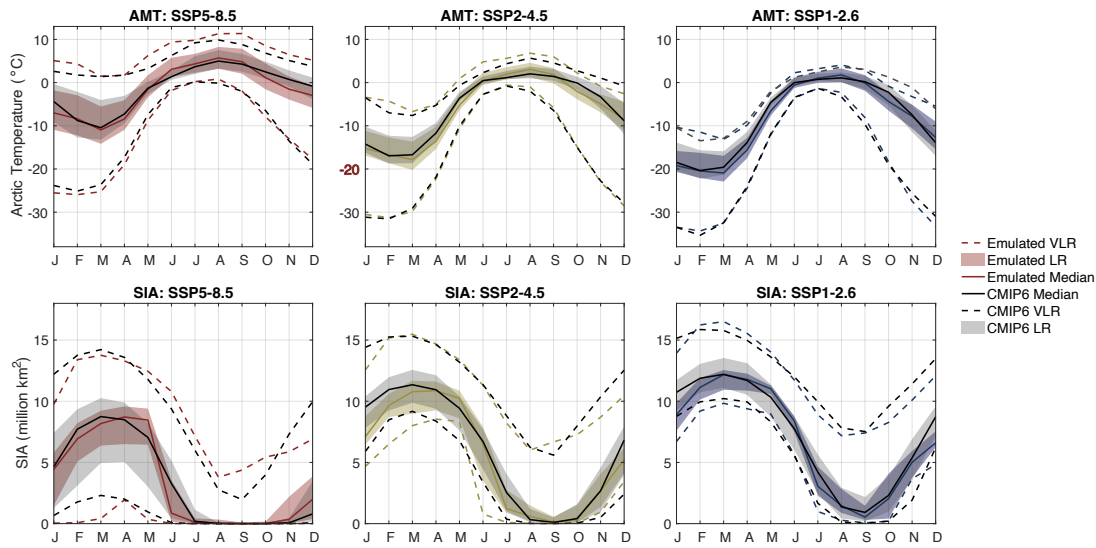

Figure B4. Comparison of our CMIP6 calibrated Arctic annual temperature cycle (top row) and Arctic SIA annual cycle (bottom row) from our CMIP6 calibrations with the equivalent CMIP6 range. Red, yellow and blue shading represents the 2080-2100 mean *likely* range from SSP5-8.5, SSP2-4.5 and SSP1-2.6 respectively. Grey shading represents the CMIP6 *likely* range. Solid red, yellow and blue lines represent the mean of our CMIP6 calibrated range. Dashed lines represent the CMIP6 calibrated *very likely* range.

When comparing the *likely* (17-83%) range of our emulated Arctic annual mean temperatures (stage i) with the *likely* range of their CMIP6 counterparts (fig. 2), it is clear a simple linear regression produces a relatively sufficient fit as all calibrated models and scenarios fall within the 95% confidence band of the CMIP6 counterpart.

705   Further statistical analysis shows that our emulator yields well calibrated parameter sets to replicate the CMIP6 seasonal Arctic temperature and SIA in SSP scenarios SSP1-2.6, SSP2-4.5 and SSP5-8.5 (fig. B4). The mean of the 2080-2100 CMIP6 multi-model distribution of the seasonal Arctic temperature cover the range -20.4°C (March) to 1.03°C (August), with a standard deviation range between 1.02 and 6.27 (Supplementary tables. A4 and A5). In comparison the sample mean produced from our emulation over the same period covers the range -20.9°C (March) to 1.12°C (August), with a standard deviation between

710   1.50 and 6.79. For our SIA parameterisation, our emulated mean covers the range 12.1 million km^2 at its maximum in March to 1.33 million km^2 at its minimum in September, with a standard deviation range between 2.34 and 1.49. The CMIP6 model distribution matches our emulation well with a range of mean SIA over this time between 12.4 million km^2 (March) and

51

1.51 million km^2 (September), with a standard deviation range between 2.42 and 1.45. Both ranges of the mean and standard deviation of our emulator significantly overlap their CMIP6 counterpart in both the temperature and SIA parameterisation, suggesting that our model's emulation is reasonably accurate in capturing the variability seen in the CMIP6 multi-model distribution. To evaluate the significance of the seasonal variances between our emulation of both variables and the CMIP6 counterpart, we use the Levene's test on the standard deviation of both the emulated and CMIP6 2080-2100 multi-model distribution (Supplementary tables. A4 and A5). When doing so we generate a p-value of 0.95 and 0.6, and an F-value of 0.0036 and 0.3 for our Arctic seasonal temperature and SIA emulations respectively.

The nuances between CMIP6 models suggest that our emulation of some models perform better than others in terms of how well they reproduce their CMIP6 counterpart. In both the seasonal temperature and SIA calibration, the models ACESSS_CM2 and CESM2 show a slightly degraded quality in terms of fit, especially in the month May. In general, we find May to be the worst fitting month in terms of both temperature and SIA, as our emulated May temperature does not increase as fast as its CMIP6 counterpart and therefore simulates too little SIA lost per degree of warming. When we remove May from our statistical evaluation, the p and F-values from our SIA projections change to 0.9 and 0.02 respectively, indicating a significantly increased fit when May is not accounted for. However overall, all other months fall within the 95% confidence band of the CMIP6 counterpart, when simply comparing the average 2080-2100, *very likely* (5-95%) and *likely* (17-83%) range. The emulated median of both variables also closely matches the CMIP6 counterpart with an R-squared value of 0.9, indicating our calibration produces a near-optimal emulation of the first ensemble CMIP6 multi-model range of all SSP scenarios.
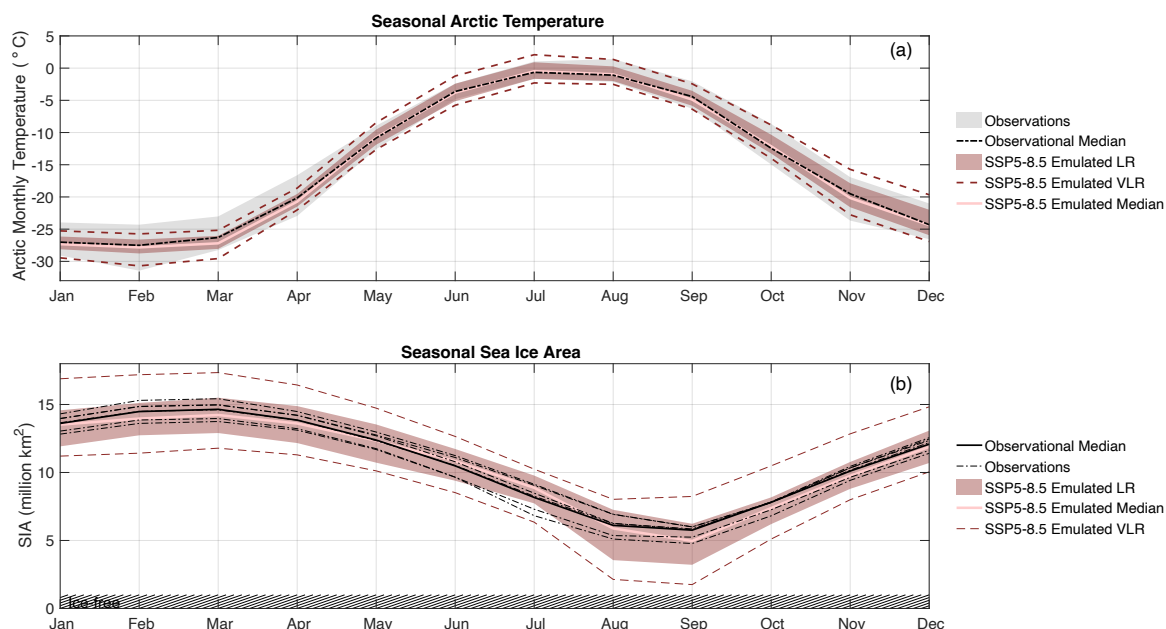
B3   How well Our Emulator Reproduces Current Seasonal Temperature Trends?

Figure B5. Comparison of our observationally constrained Arctic annual temperature cycle (top panel) and Arctic SIA annual cycle (bottom panel), with the 'plausible range' from observations. Red shading shows our calibrated 1979-2014 mean *likely* range. Dashed red lines denote the *very likely* calibrated range. Solid red lines denote the calibrated median. Grey shading represent the mean 1979-2014 *likely* range from observations. Dashed black lines denote individual observations and solid black lines denote the observational mean.

After constraining our emulator to observations, we find that our emulator is able to sufficiently capture the observed Arctic seasonal temperature cycle, when comparing the 1979-2014 *very likely* (5-95%) and *likely* (17-83%) emulated range with the observed (fig. B5). The unconstrained median 1979-2014 temperature cycle shows a positive bias between January and August with temperatures on average 1.92°C higher than the observed over this time (fig. B6). After applying the observational constraints, these biases reduce to 0.063°C, where the observed and constrained median Arctic seasonal temperature cycle show an R-squared correlation of 0.98 and an RSS goodness of fit value of 0.0636. When specifically comparing the emulated July and August temperatures to the observed, we find that after adding the bias corrections to our temperature parameterisation Eq. (3b), our summer temperatures increase at the same rate as the observed median. We therefore find that our projections reproduce the observational Arctic warming in all months, within the 95% confidence of observations.
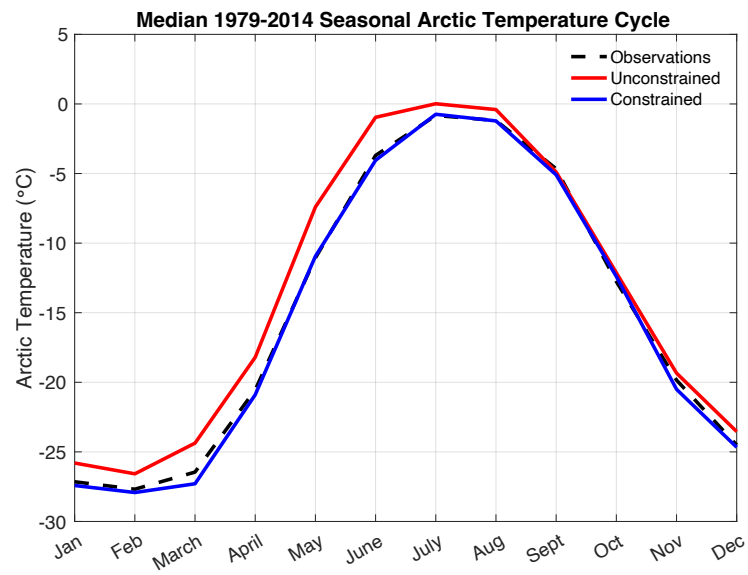
Figure B6. Comparison of the median 1979-2014 observationally constrained seasonal Arctic temperature cycle with our unconstrained CMIP6 calibrated median 1979-2014 seasonal Arctic temperature cycle. Red solid lines represent our unconstrained CMIP6 calibration, blue solid lines represent our observationally constrained emulator and black dashed lines show its comparison to observations.